

UNIVERSIDAD SAN FRANCISCO DE QUITO
USFQ

Colegio de Ciencias e Ingenierías

Estimation of maximum propagation distance of
Magnetostatic Forward Volume Waves

Proyecto de Investigación

Carolina Rocío Campuzano Páez

Licenciatura en Física

Trabajo de titulación presentado como requisito
para la obtención del título de
Licenciada en Física

Quito, 13 de mayo de 2016

UNIVERSIDAD SAN FRANCISCO DE QUITO USFQ

Colegio de Ciencias e Ingenierías

HOJA DE CALIFICACIÓN DE TRABAJO DE TITULACIÓN

**Estimation of maximum propagation distance of Magnetostatic
Foward Volume Waves**

Carolina Rocío Campuzano Páez

Calificación

Vincent Vlaminck, PhD.

Firma del profesor

Quito, 13 de mayo de 2016

Derechos de Autor

Por medio del presente documento certifico que he leído todas las Políticas y Manuales de la Universidad San Francisco de Quito USFQ, incluyendo la Política de Propiedad Intelectual USFQ, y estoy de acuerdo con su contenido, por lo que los derechos de propiedad intelectual del presente trabajo quedan sujetos a lo dispuesto en esas Políticas.

Asimismo, autorizo a la USFQ para que realice la digitalización y publicación de este trabajo en el repositorio virtual, de conformidad a lo dispuesto en el Art. 144 de la Ley Orgánica de Educación Superior.

Firma del estudiante: _____

Nombre: Carolina Rocío Campuzano Páez

Código: 00101735

Cédula de identidad 171625721-5

Lugar y fecha Quito, mayo de 2016

ACKNOWLEDGMENTS

To all my teachers who have guided me through all my college years, specially to Vincent for his help in the realization of this work. To all my family and friends for their unconditional support.

RESUMEN

Las ondas de spin ofrecen una herramienta para la mejora de dispositivos de Spintrónica. Las ondas con carácter propagativo se pueden utilizar en múltiples dispositivos que incluyen inducción y detección de ondas de spin para diferentes distancias. Simulando la respuesta inductiva de las ondas de spin que se propagan a través de una lámina ferromagnética delgada podemos estudiar su distancia de atenuación. Presentamos un cálculo basado en la teoría de ondas magnetostáticas junto con un término de amortiguamiento de Gilbert. Para estudiar la máxima distancia de propagación simulamos los resultados que se podrían obtener durante un experimento de Propagating Spin wave Spectroscopy mediante un modelo que considera las ecuaciones de Maxwell en la configuración experimental. La simulación utiliza un algoritmo de optimización para determinar la distancia de amortiguamiento para un amplio rango de vectores de onda $k = [1 \dots 12, 5] \mu m^{-1}$ y frecuencias $f = [5 \dots 20] GHz$. Presentamos resultados para el primer modo de propagación, Magnetostatic Forward Volume Wave, para una lámina de Permalloy considerando la sensibilidad de detección de el aparato de medición (10 fH). Este trabajo sirve como referencia para la optimización del diseño de dispositivos experimentales.

ABSTRACT

Spin waves offer a tool for improving spintronics devices. Propagative waves can be used into several devices that include both excitation and detection of spin waves for different distances. By simulating the inductive response of spin waves propagating through a thin ferromagnetic strip we study spin waves attenuation lengths. We present a calculation based on magnetostatic wave theory combined with the Gilbert form of the damping. To study attenuation distances we simulate the results that could be obtained using Propagating Spin wave Spectroscopy by implementing a model that considers Maxwells equations for this experimental configuration. The simulation uses an optimization algorithm to determine the maximum propagation distance of a broad range of wave vector $k = [1 \dots 12, 5] \mu m^{-1}$ and frequency $f = [5 \dots 20] GHz$. We represent results for the Magnetostatic Forward Volume Wave mode in a Permalloy strip, obtained considering the detective threshold of an actual measuring device (10 fH). This work serves as a reference for optimizing design of experimental devices.

Contents

1	Static Magnetism	9
1.1	Different magnetic materials	9
1.2	Magnetic Interactions	10
1.2.1	Exchange Interaction	11
1.2.2	Magnetocrystalline Anisotropy	12
1.2.3	Dipolar Interaction	12
1.2.4	Zeeman term interaction	13
1.2.5	Effective Field	14
2	Magnetization Dynamics	15
2.1	Uniform Dynamics	15
2.1.1	Landau-Lifschitz equation	15
2.1.2	Linear response to an excitation	15
2.1.3	Uniform resonance for an ellipsoid	17
2.1.4	Uniform resonance for different geometries	19
2.2	Non Uniform dynamics	20
2.2.1	Magnetostatic approximation for volume waves	20
2.2.2	Magnetostatic waves in a thin film	23
2.3	Phenomenological approach of damping	26
3	Propagating Spin wave Spectroscopy	28
3.1	Description of the technique	28
3.2	Spin wave transduction model	29
3.2.1	Inductance of the antennas	29
3.3	Fourier Transform of the antenna	32
4	Simulation of the MsFVW	34
4.1	Self inductance inductance spectra	35
4.2	Mutual inductance spectra	37
4.2.1	Attenuation length	38
4.3	Determination of the maximum propagation length	40
5	Conclusions	42
6	References	43

Introduction

Magnetic excitations in solids at microwave frequencies has been a topic of study for several decades due the particularities displayed by spin waves. Spin waves in contrast with other waves have a dispersion relation governed by magnetic interactions, mainly dipolar and exchange. Other interesting properties of spin waves are that they exist in a microwave frequency spectrum and they have low group velocities. In particular, in the 1960s microwave technology implemented spin wave devices such as circulators and analog delay lines. Modern spin wave technology nowadays mainly focuses in routing and processing electrical signals.

The replacement of electric current by other physical mechanisms such as magnetostatic waves or exchange spin waves appears as a potential field of study. Recently there have been several attempts to employ magnetic phenomena for performing logical operations [15]. The goal of these studies is to use spin waves in analog computing, but it can be extended into digital signal technology since spin wave signal conversion into digital has been theoretically proposed [21]. A first working spinwave based logic circuit has been experimentally demonstrated by M. Kostylev [16]. Logic gates have been manufactured using propagating spin-wave in an interferometer geometry [20, 19]. Moreover, information can be coded into a spin wave phase and transmitted through a magnetic film by propagation (Spin Wave Bus) [20].

In this work we study, for an broad range of wave vector and frequency, the maximum propagation distance for the Magnetostatic Foward Volume Wave in a thin ferromagnetic film. To do so, we present simulated spin wave spectra obtained using a model adapted from the Propagating Spin Wave Spectroscopy (PSWS) technique.

The manuscript is organized as follows. First, the useful tools of static magnetism are reviewed in chapter 1, this allows to comprehend spin wave dynamics that are presented in chapter 2. Next, the PSWS technique is presented, with an electromagnetic model that reproduces closely the experimental conditions, in chapter 3. We then present the results on the feasibility of spin wave maximum propagation distance.

1 Static Magnetism

Magnetism in matter displays a large variety of behaviors, which result, from the interplay of the different magnetic interactions. In this chapter, we will briefly discuss the different magnetic materials and their properties, the main magnetic interactions and the effective fields.

1.1 Different magnetic materials

Magnetism in the atom has a quantum origin. The magnetic moment \vec{m} of the atom is related to the total angular momentum \vec{j} :

$$\vec{m} = \gamma \vec{j} \quad (1.1)$$

where $\gamma = -\frac{ge}{2m_e}$ is the gyromagnetic ratio, the negative sign indicates that the magnetic moment and the angular momentum are anti-parallel due to the electron's negative charge [2]. The g factor in γ depends on the environment, in the special case of a free electron $g = 2$ and $\gamma = 27,9 \text{ GHz T}^{-1}$, which justifies the microwave domain of magnetic excitation. The magnetic moment of the atom can also be visualized using classical mechanics, the Bohr atomic model offers the opportunity of describing the atom using orbital motion. Bohr's magneton μ_B is the value of the magnetic moment of the atom considering that the electron orbits the atom just as in Bohr's model. ($\mu_B = \frac{e\hbar}{2m_e}$). Using this approach equation (1.1) can be rewritten:

$$\vec{m} = \frac{\mu_B g}{\hbar} \vec{j} \quad (1.2)$$

Since each atom in the material has an individual magnetic momentum, it is convenient to use a semi continuous approach; in this approach the magnetic moment of the atom can be visualized as a dipole, and matter can be understood as a large arrange of this dipoles. Since the arrangement is large it is useful to define a density of magnetic moments called magnetization, \vec{M} , described as

$$\vec{M} = \frac{\sum_V \vec{m}}{V} \quad (1.3)$$

where V is a mesoscopic volume.

Due to different magnetic interactions, which we will study in more detail later, the magnetization displays different responses in the presence of an applied field. In order to classify them we introduce the magnetostatic susceptibility tensor $\bar{\chi}$ which contains the information of the different magnetic interactions.

$$\vec{M} = \vec{M}_0 + \bar{\chi} \cdot \vec{H}_{ext} \quad (1.4)$$

Where \vec{H} is assumed small and M_0 is the magnetization in the absence of an applied

field [3].

We classify the different types of magnetic materials based on this response, they can be diamagnetic, paramagnetic, ferromagnetic, antiferromagnetic, and ferrimagnetic.

Diamagnetic materials react to the external field by aligning their dipoles against the applied field, therefore creating a magnetization opposite to \vec{H} . Usually diamagnetic response is weak, values of χ are usually in the order of 10^{-5} . The origin of diamagnetism is a modification of the electron's orbit in response to the external field, therefore this effect is present in any material (although it is weak). Typical diamagnetic materials are water, Mercury, pyrolytic Carbon and Bismuth.

Paramagnetic materials are those that place the magnetic moments parallel (by rotating the spins) to the applied field and therefore create a magnetization parallel to it [2]. For these substances there is no net magnetization when $H_{ext} = 0$.

Ferromagnetic materials. Some materials possess a permanent magnetization even in the absence of a field, they are called ferromagnetic. This order only exists below a critical temperature (T_C) above which the thermal energy dominates and produces a disordered state. Common examples of ferromagnets are Cobalt ($T_C = 1388 K$), Iron ($T_C = 1043 K$), Permalloy ($Fe_{20}Ni_{80}$) ($T_C \approx 600 K$) and Nickel ($T_C = 627 K$) [5, 18]. Long range magnetic order due to the interaction between spins favors a parallel alignment between them.

Antiferromagnetic materials. If the magnetic moments are anti parallel with the nearest neighbor and the magnitude of those pointing upwards is equal to the magnitude of those pointing downwards the material is antiferromagnetic. Since the magnitude of dipoles pointing upwards and downwards are equal there will be no spontaneous magnetization [2].

Ferrimagnetic materials. Finally, if magnetic moments are anti parallel with their nearest neighbor and the number of the dipoles pointing in one direction is not the same as those pointing in the opposite direction the material is ferrimagnetic [2]. Another possibility for ferrimagnetism is that all spins are oriented in the same direction, but the magnitude of one atom magnetic moment is different than its nearest neighbor. These materials can have positive or negative spontaneous magnetization according to the substance.

1.2 Magnetic Interactions

Magnetic interactions refer to the influence that one magnetic moment has on its neighbors. The magnetic moments create internal fields, and therefore contribute to the internal energy of the material. The interactions have different origins; they can depend on the nearest neighbor distance (exchange interaction), on the crystalline structure (magnetic anisotropy), on the macroscopic shape (dipolar interaction) and on the external fields (Zeeman effect).

1.2.1 Exchange Interaction

The idea of a molecular field which is proportional to the magnetization was first introduced by Pierre Weiss in 1906 [5]. This molecular field is occasioned by the position and motion of electronic spin states by electrostatic interaction and the Pauli exclusion principle. Both motion and orientation of an electron spin are influenced by nearby electrons, therefore the spins are correlated and they contribute to the energy as shown.

$$E_{ij}^{(ex)} = -2J_{ij}\vec{S}_i \cdot \vec{S}_j \quad (1.5)$$

Where i and j are two interacting spins and J_{ij} is the exchange integral. If the energy value is positive, then the lowest energy state is parallel alignment; if it is negative, then the lowest energy state is anti-parallel alignment. Usually the value of J_{ij} decreases rapidly with distance, for this reason exchange interaction has a short range.

When considering a large arrange of atoms, it is necessary to sum over all the atoms in the sample; the energy of the entire structure is:

$$E_{ex} = -2 \sum'_j J_{ij} \vec{S}_i \cdot \vec{S}_j \quad (1.6)$$

where \sum'_j represents the sum over the nearest neighbors of j .

An approachable interpretation of exchange interaction can be understood by visualizing the magnetic moments joined together with a spring. A sketch of this approach is presented on figure (1.1 a); in the graph the spring is connected only to the nearest neighbor because the exchange interaction has a short range. As one magnetic moment tends to change its orientation (due to thermal energy for example), the exchange interactions brings it to its original position.

Taking into account the Hamiltonian and the spring like interaction we derive the exchange field:

$$\vec{H}_{ex} = \frac{2ZJ_{ij}}{g^2N\mu_0\mu_B^2}\vec{M} + \frac{2A_{ex}}{\mu_0M_s^2}\nabla^2\vec{M} \quad (1.7)$$

where A_{ex} is the exchange constant of the material, M_s is the saturation magnetization (maximum magnetization), Z is the number of nearest neighbors, and N is the density of moments. In the latter expression, the first term is related to uniform magnetization and the second one to non-uniform one. It is notable that the first term could be neglected if we take the zero of energy when the magnetization is uniform.

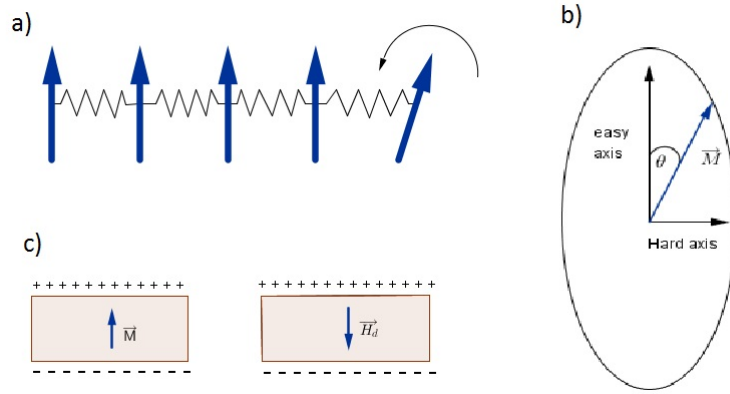


Figure 1.1: Different magnetic interactions

1.2.2 Magnetocrystalline Anisotropy

Substances such as $3d$ ferromagnetic elements have a privileged direction for the magnetization to align due to their crystal structure; this direction is called an easy axis [3]. On the other hand, some directions take more energy than others; these are called hard directions. The energy due to this interaction in the case of a uniaxial anisotropy axis is:

$$E_a = K_1 \sin^2 \theta \quad (1.8)$$

where θ is the angle between the magnetization and the easy axis, as seen in figure (1.1 b), and K_1 is the anisotropy constant. Materials where K_1 is negative tend to locate the magnetization perpendicular to the easy axis. If K_1 is positive the lowest energy occurs when the magnetization is parallel or anti-parallel to the preferential axis.

The anisotropy field H_a is defined as the field needed to saturate the magnetization of a uni-axial crystal in a hard direction [3]:

$$\vec{H}_a = -\frac{1}{\mu_0} \nabla_{\vec{M}} (E_a) \quad (1.9)$$

Typical values of the anisotropy field range between 0 and $20 \cdot 10^6 \text{ Am}^{-1}$ [3].

1.2.3 Dipolar Interaction

All materials have boundaries which represent a drastic change in magnetization; at the surface of the sample, the magnetization suddenly disappears [2]. On the surface of the material, magnetic moments are left as if they were local “monopoles” and they create a demagnetizing field. Figure (1.1 c) shows a sketch that represents the accumulation of the “magnetic charges” on a thin film magnetized perpendicularly to a plane. It is important to note that the induced field is opposite to the magnetization, that is why this field is called demagnetizing.

The demagnetizing field can be written:

$$\vec{H}_d = -\mathbb{N}\vec{M} \quad (1.10)$$

where \mathbb{N} is the demagnetizing tensor that meets the condition [2]:

$$\mathbb{N}xx + \mathbb{N}yy + \mathbb{N}zz = 1 \quad (1.11)$$

The susceptibility tensor is diagonal and responds to the macroscopic geometry of the sample. For example, for the case illustrated on figure (1.1 c) of an infinite plane, choosing the z axis as the one gives $\mathbb{N}xx = 0$ $\mathbb{N}yy = 0$ $\mathbb{N}zz = 1$, when \vec{M} and the dipolar field are perpendicular to the plane.

The energy associated to the demagnetizing field is [2]:

$$E_d = -\frac{\mu_0}{2} \int_V \vec{M} \cdot \vec{H}_d dV \quad (1.12)$$

It is important to remark that since the dipolar field is opposite to the magnetization the energy is positive, therefore the lowest energy configuration avoids the creation of these fields.

A useful result, that we will use later, is the one given for an ellipsoid with its long axis along the z axis:

$$\mathbb{N}xx = \frac{b}{b+a}; \quad \mathbb{N}yy = \frac{a}{b+a}; \quad \mathbb{N}zz = 0 \quad (1.13)$$

where a and b are the longer and shorter semi axis respectively [5].

1.2.4 Zeeman term interaction

Zeeman interaction is the mechanism that allows an external magnetic field to change the energy of a magnetic moment $\vec{\mu}$. The Zeeman energy is:

$$E_{Zeeman} = -\vec{\mu} \cdot \vec{B} \quad (1.14)$$

where \vec{B} is the external magnetic field [3]. When an external field is applied to a material, Zeeman interaction is responsible for aligning the magnetic moment with an external field; the energy due to this interaction on a sample is [3]:

$$E_z = -\mu_0 \int_v \vec{B}_{ext} \cdot \vec{M} dV \quad (1.15)$$

The negative sign in the latter equation means that the lowest energy occurs when both magnetization and field are parallel.

1.2.5 Effective Field

Magnetic interactions produce an effective magnetic field which is the superposition of all interaction's fields.

$$\vec{H}_{eff} = \vec{H}_a + \vec{H}_{ext} + \vec{H}_{ex} + \vec{H}_d \quad (1.16)$$

The effective field is a the result of a competition between all interactions. Also, the energy is a superposition of all interaction terms.

$$E = E_z + E_d + E_a + E_{ex} \quad (1.17)$$

The result of the competition between interactions determines the equilibrium configuration for the magnetization.

A specially useful comparison between magnetic interactions is between dipolar and exchange fields. The exchange length (l_{ex}) is the distance at which the exchange interaction is overwhelmed by the dipolar one.

$$l_{ex} = \sqrt{\frac{2A_{ex}}{\mu_0 M_s^2}} \quad (1.18)$$

When introducing the concept of exchange length we can rewrite the second term in equation (1.7) as $\vec{H}_{ex} = l_{ex}^2 \nabla^2 \vec{M}$ [2].

Another noteworthy observation about the competition between magnetic interactions has to do with domain formation. Exchange interaction and magneto-crystal anisotropy favor a particular direction of spin configuration, named mono domain; but this configuration creates an energetically unfavorable radiating dipolar field. The creation of multiple domains, illustrated on figure (1.2 b and c), allows the magnetic flux, created by dipolar field, to close some of the radiated flux and therefore lowers the energy. Exchange interaction increases the energy with multiple domain formation due to rapid change of spin orientation in domain walls. This competition between dipolar and exchange interaction determines the materials most energetically favorable configuration.

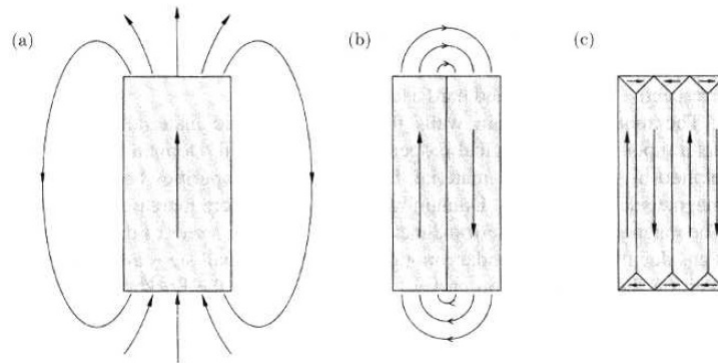


Figure 1.2: Multiple domains [2]

2 Magnetization Dynamics

On this section, we will discuss the motion of the magnetic moments in girotropic media. First we will address the case of uniform magnetization ($k = 0$), and present the case of an ellipsoid and other basic geometries. Then we will discuss non uniform dynamics ($k \neq 0$); where we will describe the magnetostatic approximation for volume waves. Finally, we will discuss the phenomenological approach of the damping.

2.1 Uniform Dynamics

2.1.1 Landau-Lifschitz equation

Dynamics in ferromagnets can be described using the continuum approach that allows one to use a classic mechanical view. We can consider a region of uniform magnetization as a macro-spin. Classically, the angular momentum rate of change is equal to the torque exerted to the particle's momentum. We take a small but macroscopic volume ΔV and its angular momentum \vec{J} , and sum over the volume, which leads to the well-known Landau Lifschitz equation:

$$\frac{\partial \vec{M}}{\partial t} = -\gamma \mu_0 \vec{M} \times \vec{H}_{eff} \quad (2.1)$$

which describes the motion of \vec{M} in the absence of dissipation of magnetic energy. We will discuss the damping in section **2.3**. It is interesting to remark that this equation does ensure the conservation of the vector \vec{M} length, namely multiplying both sides of the latter equation scalarly by \vec{M} , we obtain

$$\frac{\partial}{\partial t} M^2 = 0 \quad (2.2)$$

Therefore, the head of \vec{M} moves on a sphere of radius M_s .

2.1.2 Linear response to an excitation

We will now use the equation of motion to describe the position of the magnetization by assuming that there is a linear response to an excitation field.

We will assume that the fields and magnetization can be described as a static equilibrium component plus a small time dependent perturbation, [3]

$$\vec{H}_{eff} = \vec{H}_{eq} + \vec{h}(t) \quad (2.3)$$

$$\vec{M} = \vec{M}_{eq} + \vec{m}(t) \quad (2.4)$$

such that time dependent perturbation is much smaller than the static component, $|\vec{H}_{eq}| \gg |\vec{h}(t)|$ and $|\vec{M}_{eq}| \gg |\vec{m}(t)|$ as seen in figure (2.1).

In order to obtain the equilibrium condition, both magnetization and equilibrium field are put into the Landau-Lifschitz equation (2.1), since the equilibrium condition is time independent $\vec{M}_{eq} \times \vec{H}_{eq} = 0$. Therefore, the equilibrium condition is $\vec{M}_{eq} \parallel \vec{H}_{eq}$. Furthermore, since the norm of the magnetization is conserved, the time dependent perturbation must be perpendicular to the equilibrium magnetization. We will assume that the static equilibrium field and magnetization lie over the \hat{z} axis as sketched in figure (2.1).

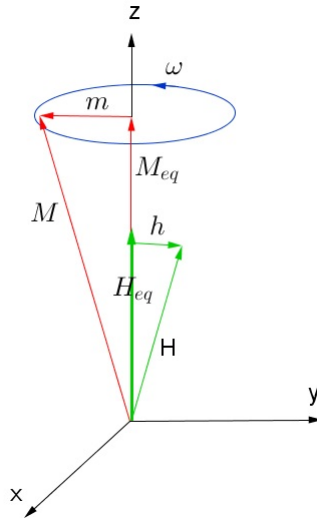


Figure 2.1: Field and magnetization configuration

The linearized expression of the Landau Lifschitz equation is obtained by keeping only the first order terms:

$$\frac{\partial \vec{m}}{\partial t} = -\gamma\mu_0 \left(\vec{M}_{eq} \times \vec{h}(t) + \vec{m}(t) \times \vec{H}_{eq} \right) \quad (2.5)$$

We look for harmonic solution in response to a sinusoidal excitation, $\vec{h}(t) = \vec{h} e^{i\omega t}$ and $\vec{m}(t) = \vec{m} e^{i\omega t}$. Then

$$(m_x \hat{x} + m_y \hat{y}) i\omega = -\gamma\mu_0 (M_{eq} \hat{z} \times (h_x \hat{x} + h_y \hat{y}) + (m_x \hat{x} + m_y \hat{y}) \times H_{eq} \hat{z})$$

after projecting

$$\begin{aligned} m_x i\omega &= \gamma\mu_0 M_{eq} h_y - \gamma\mu_0 H_{eq} m_y \\ m_y i\omega &= -\gamma\mu_0 M_{eq} h_x + \gamma\mu_0 H_{eq} m_x \end{aligned}$$

solving for m , by replacing $\omega_H = \mu_0 \gamma H_{eq}$ and $\omega_M = \mu_0 \gamma M_{eq}$ and using the definitions:

$$\chi = \frac{\omega_H \omega_M}{\omega_H^2 - \omega^2} \quad (2.6)$$

$$\chi_a = \frac{\omega \omega_M}{\omega_H^2 - \omega^2} \quad (2.7)$$

we obtain

$$\vec{m} = \overline{\chi}_p \vec{h} \quad (2.8)$$

where $\overline{\chi}_p$ is the Polder susceptibility tensor.

$$\overline{\chi}_p = \begin{bmatrix} \chi & i\chi_a & 0 \\ -i\chi_a & \chi & 0 \\ 0 & 0 & 0 \end{bmatrix} \quad (2.9)$$

The dynamic described above corresponds to a precession movement of the magnetization. Depending on the symmetry of the sample, the trajectory of \vec{m} can be circular (cylindrical symmetry), ellipsoidal (most general) and can become very complex as the amplitude of precession decreases [4].

2.1.3 Uniform resonance for an ellipsoid

As seen before, the effective field plays a crucial roll in the solution of the Landau-Lifschitz equation. In the particular case in which we can neglect magnetocrystal anisotropy and the exchange interaction, the effective field depends on the macroscopic shape of the sample due to the demagnetizing field and the demagnetizing tensor. Previously the time dependent magnetization at a certain point was calculated with a given magnetic field at the same point; however, this field usually cannot be regarded as given since it depends on magnetization distribution over the entire system [4]. Quantities as the power flux of the incident electromagnetic wave at the input of the system are the only ones that can be regarded as given [4].

The following section studies resonance considering uniform oscillations of magnetization for a *small* (in comparison with the length of electromagnetic wave in the sample) ferromagnetic ellipsoid. The ellipsoidal geometry offers the advantage that for a uniform \vec{M} we can consider only the dipolar term. A uniform magnetization gives a uniform demagnetizing field, the dipolar field is therefore the product of the magnetization and the demagnetizing tensor. We will neglect magneto-crystalline anisotropy, therefore the effective field is:

$$\vec{H}_{eq} = \vec{H}_{ext} + \vec{H}_d = \vec{H}_{ext} - N\vec{M} \quad (2.10)$$

A sketch of the fields and magnetization is shown on figure (2.2).

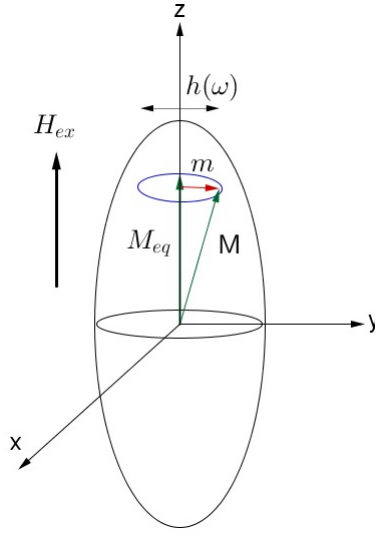


Figure 2.2: Field and magnetization on an ellipsoid

In addition, the oscillating transverse field is also affected by the demagnetizing tensor, it is:

$$\vec{h} = \vec{h}_e - \mathbb{N}_\perp \vec{m} \quad (2.11)$$

where \mathbb{N}_\perp is

$$\mathbb{N}_\perp = \begin{pmatrix} N_{xx} & 0 \\ 0 & N_{yy} \end{pmatrix} \quad (2.12)$$

Taking this into account, equation (2.10) can be rewritten as:

$$\vec{H}_{eq} = \vec{H}_{ext} - N_z \vec{M}_{eq} \quad (2.13)$$

Using the linearized solution for Landau-Lifschitz, equation (2.8), we can derive

$$\vec{h} = \overline{\chi}_p^{-1} \vec{m}$$

where

$$\overline{\chi}_p^{-1} = \frac{1}{\omega_M} \begin{pmatrix} \omega_x & i\omega \\ -i\omega & \omega_y \end{pmatrix}$$

$$\omega_x = \omega_0 + N_x \omega_m$$

$$\omega_y = \omega_0 + N_y M_{eq}$$

and $\omega_0 = \gamma \mu_0 (H_{ext} - N_z M_{eq})$. At resonance the magnetic response is supposed to be divergent, therefore:

$$|\overline{\chi}_p^{-1}| = \frac{\omega_x \omega_y - \omega^2}{\omega_M^2} = 0$$

Then, the resonance frequency is:

$$\omega_{res} = \sqrt{\omega_x \omega_y} \quad (2.14)$$

For the case of the ellipsoid (with a similar section) we get an elliptic precession:

$$\frac{m_x}{m_y} = -i\sqrt{\frac{\omega_y}{\omega_x}} \quad (2.15)$$

The latter equation reveals that the precession is not circular since ω_x is not necessarily equal to ω_y therefore the ratio is not equal to 1 as it would be the case of a circular precession.

2.1.4 Uniform resonance for different geometries

As seen on the previous section, the resonance frequency for a ferromagnet depends on the macroscopic shape of the sample. The result for the ellipsoid can be extended to certain shapes as long as the boundaries resemble an ellipsoid. For example, a long cylinder can be considered as an ellipsoid as long as it is very large in comparison with its width; a thin film can be treated as an ellipsoid as long as it is thin and large.

Table (1) presents a summary of the values of the demagnetizing coefficients for different geometries in the case of an ellipsoid. Using the demagnetizing coefficients we obtain the resonance frequencies for each basic geometry.

Sample	M direction	fig. (5)	Demag. factors			Resonance Frequency
			N_x	N_y	N_z	
Thin plate	Tangential	(a)	0	1	0	$\left(\frac{\omega_0}{\gamma}\right)^2 = H_{eq}(H_{eq} + M_{eq})$
	Normal	(b)	0	0	1	$\frac{\omega_0}{\gamma} = H_{eq} - M_{eq}$
Thin Slab	Longitudinal	(c)	$\frac{1}{2}$	$\frac{1}{2}$	0	$\frac{\omega_0}{\gamma} = H_{eq} - \frac{1}{2}M_{eq}$
	Transverse	(d)	$\frac{1}{2}$	0	$\frac{1}{2}$	$\left(\frac{\omega_0}{\gamma}\right)^2 = H_{eq}(H_{eq} - \frac{1}{2}M_{eq})$
Sphere		(e)	$\frac{1}{3}$	$\frac{1}{3}$	$\frac{1}{3}$	$\frac{\omega_0}{\gamma} = H_{eq}$

Table 1: Frequencies of ferromagnetic resonance in small samples [4]

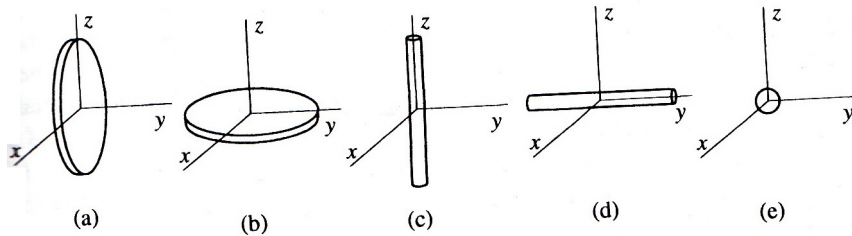


Figure 2.3: Limiting cases of an ellipsoid [4]

Precession is usually detected by resonant absorption of microwaves and it is necessary that high-frequency radiation penetrates the sample. For metallic iron at 10 GHz the skin depth (depth of penetration of the electromagnetic field into the substance)

is in the order of a micron, for this reason thin films are a common sample in metallic materials [5].

2.2 Non Uniform dynamics

In the case of non uniform excitations, the magnetic perturbation propagates in the form of a spin wave. As sketched on figure (2.4), spin wave is a continuous phase shift of the magnetic moments precession along the propagation direction, a sketch is presented in figure (2.4). In this section we will study spin waves using the magneto-static approximation for volume waves in an unbounded region. We will consider only dipolar interaction as we will see that exchange interaction does not affect the dispersion relation for the wave vector range that we study and adopt a phenomenological approach for the case of thin films. We will assume that the wavelength of the magnetostatic wave must be large in comparison with the exchange interaction distance ($\lambda \gg l_{ex}$); typical exchange length values are in the order of nano meters, in particular, for Permalloy $l_{ex} = 5,7 \text{ nm}$ [18].

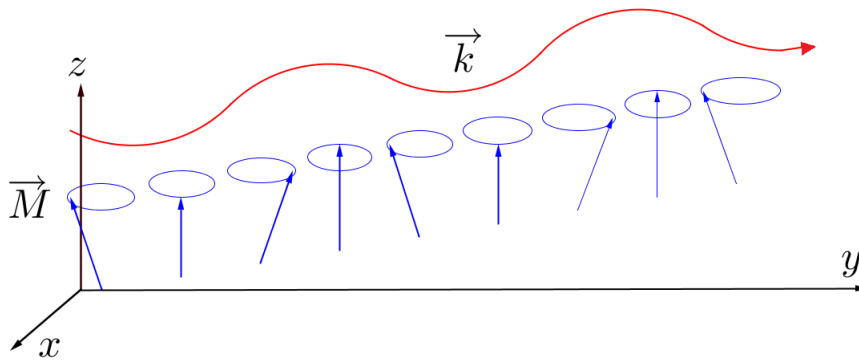


Figure 2.4: Spin wave

2.2.1 Magnetostatic approximation for volume waves

In order to describe electrodynamics in isotropic media and an unbounded region, we must use Maxwell's general equations and boundary conditions. Maxwell's equations for a magnetic field composed by the superposition of a steady and an oscillating field are [4]:

$$\begin{aligned}\nabla \times \vec{e} + ik_0 \bar{\mu} \vec{h} &= \vec{0} \\ \nabla \times \vec{h} - ik_0 \bar{\epsilon} \vec{e} &= \frac{4\pi}{c} \vec{j}_{ext} \\ \nabla \cdot (\bar{\mu} \vec{h}) &= 0 \\ \nabla \cdot (\bar{\epsilon} \vec{e}) &= 4\pi \rho_{ext}\end{aligned}$$

where $\bar{\mu} = \mu_0 (\mathbb{I}_d + \overline{\chi_p})$ and $k_0^2 = \omega^2 \mu_0 \epsilon$ is the electromagnetic wave vector. For the case in which we will be working, there are no free charges neither free currents; therefore, $\vec{j}_{ext} = \vec{0}$ and $\rho_{ext} = 0$. Moreover, we will consider uniform plane waves for electric and magnetic field, $\vec{e} = \vec{e}_0 e^{i(\vec{k} \cdot \vec{r} - \omega t)}$ and $\vec{h} = \vec{h}_0 e^{i(\vec{k} \cdot \vec{r} - \omega t)}$; meaning that the magnetic field depends only in one coordinate which is the propagation direction. By replacing \vec{e} and \vec{h} in Maxwell's equations:

$$\vec{k} \times \vec{e} = \omega \mu_0 (\mathbb{I}_d + \overline{\chi_p}) \vec{h} \quad (2.16)$$

$$\vec{k} \times \vec{h} = -\omega \bar{\epsilon} \vec{e} \quad (2.17)$$

$$\vec{k} \cdot \vec{b} = 0 \quad (2.18)$$

$$\vec{k} \cdot \bar{\epsilon} \vec{e} = 0 \quad (2.19)$$

By taking the rotational of equation (2.16) and using equation (2.17) we derive [4]:

$$\vec{k} \times \vec{h} = \frac{k_0^2 \vec{k} \times \overline{\chi_p} \vec{h}}{(k^2 - k_0^2)} \quad (2.20)$$

The term k_0 corresponds to the propagation constant of the electromagnetic waves in the absence of gyromagnetic effects ($\chi = 0$) where \vec{k} is the spinwave vector. In the case of ferromagnetic resonance the frequency of the electromagnetic waves varies between $1 - 100 \text{ GHz}$ therefore the typical value of k_0 is about $1 - 100 \text{ cm}^{-1}$. For k values larger than 100 cm^{-1} . the rotational of \vec{h} can be taken as 0:

$$\vec{\nabla} \times \vec{h} = 0 \quad (2.21)$$

$$\vec{\nabla} \cdot \bar{\mu} \vec{h} = 0 \quad (2.22)$$

Since the rotational of \vec{h} is null, one can express \vec{h} as a gradient of a scalar function ψ called the magnetostatic potential, $\vec{h} = \vec{\nabla} \psi$; this is what is called the magnetostatic approximation. By replacing the last expression into Maxwell-flux equation, we can write

$$\vec{\nabla} \cdot \mu_0 (\mathbb{I}_d + \overline{\chi_p}) \vec{\nabla} \psi = 0 \quad (2.23)$$

The latter expression is called the Walker equation. For the case of a plane wave in the volume, we will write a periodic magnetostatic potential

$$\psi(\vec{r}, t) = \psi_0 e^{i(\omega t - \vec{k} \cdot \vec{r})} \quad (2.24)$$

The Walker equation is solved simply by derivating ψ and multiplying by the magnetic susceptibility, using the gradient operator again, equation (2.23) reduces to

$$(1 + \chi) (k_x^2 + k_y^2) + k_z^2 = 0 \quad (2.25)$$

We define θ_k as the angle between \vec{M}_0 and \vec{k} , such that $\tan^2(\theta_k) = \frac{k_x^2 + k_y^2}{k_z^2}$, therefore equation (2.25) is:

$$1 + \chi = -\cot^2(\theta_k)$$

Since we have neglected exchange, we use the definition of χ given in equation (2.6). By doing this we get $1 + \chi = -\frac{k_z^2}{k_x^2 + k_y^2} = -\frac{1}{\tan^2\theta}$, therefore the dispersion relation is:

$$\omega^2 = \omega_H (\omega_H + \omega_M \sin^2\theta_k) \quad (2.26)$$

for the spin wave induced in the unbounded region. The angle θ_k is in the interval $[0, \frac{\pi}{2}]$ for that $\chi < 0$, therefore the precession frequency is restrained to this values

$$\omega_H \leq \omega \leq \sqrt{\omega_H^2 + \omega_M \omega_H} \quad (2.27)$$

The latter equation gives the frequency band for magnetostatic volume waves.

It is important to note that the frequency of the magnetostatic waves in an unbounded region depends on the direction of propagation but not on the amplitude of the wave vector, therefore the group velocity is equal to zero. Since the group velocity is null there is no energy flux in the wave, they are stationary waves.

Finally we will now show that the exchange interaction leads to a propagative character of the volume spin wave although it factors only for very high wave vectors. The exchange field depends on the laplacian of the magnetization as seen in equation (1.7), taking into account that $m = m_0 e^{i(\omega t - \vec{k} \cdot \vec{r})}$ we can rewrite the exchange field

$$\vec{h}_{ex} = -\frac{2A_{ex}}{\mu_0 M_s^2} k^2 \vec{m} \quad (2.28)$$

which leads to the substitution $\omega_H \rightarrow \omega_H + \eta k^2$ in the linearized equation of Landau-Lifshitz (2.5), where $\eta = \gamma \frac{2A_{ex}}{\mu_0 M_s^2}$. By following the same process as in section 2.3.1 we arrive to a dispersion relation that takes in count the exchange interaction

$$\omega^2 = (\omega_H + \eta k^2) (\omega_H + \eta k^2 + \omega_M \sin^2\theta_k) \quad (2.29)$$

This dispersion relation shows that the group velocity is different and greater than zero.

On the other hand, the dipolar field is approximately $h_d \approx m$ since the demagnetizing factors are normalized. For us to neglect exchange interaction the dipolar field must be greater than the exchange one, then:

$$k < k_{max} = \sqrt{\frac{\mu_0 M_s^2}{2A_{ex}}}$$

For this work the material selected is Permalloy for which $A_{ex} = 1,3 \cdot 10^{-13} \text{ Jm}^{-1}$

and $M_s = 0,1693 T$ [18], therefore the maximum k vector allowed is $1,86 \times 10^9 m^{-1}$ which corresponds to a wavelength $\lambda = 3,37 nm$. So we will easily ignore the exchange term to describe the propagation of spin waves for the range of wave vector considered $k = [0,5 \dots 12,5] \mu m^{-1}$.

2.2.2 Magnetostatic waves in a thin film

As an effect of non-uniform excitation, magnetostatic waves are induced in a sample. When studying spin waves we must take into account that it is impossible to have an unbounded region as the one considered above, for this reason we will focus on magnetostatic waves on a thin film. The propagative character of magnetostatic waves comes from the boundary conditions. We will use a phenomenological approach to describe spin waves and to describe how the phase of the magnetic moment is traveling in a determined direction [4]. A spin wave in a thin film can be approximated as a sequence of mesoscopic volumes as sketched on figure (2.5). We will make a very simple approximation that the film can be divided into $\lambda/4$ segments that have uniform magnetization. The different segments induce magnetic “charges” in their boundaries that generate a dynamic dipolar field which is responsible of the wave propagation. The spin precesses along the z axis; as seen on the sketch, there is a $\pi/2$ dephase in the spins angle between one mesoscopic volume and the following.

Magnetostatic Foward Volume Waves The configuration shown in figure (2.5) where the k vector lies along the main axis of the film and the equilibrium magnetization is perpendicular to the plane of the film. This configuration is called magnetostatic forward volume wave (MsFVW). In order to calculate the correspondent dipolar field we will assume that the $\lambda/4$ segments are ellipsoids.

For this configuration the “charges” are induced in the planes were the wave propagates. By analyzing the demagnetizing coefficients that were described in equation (1.13) and taking the thickness t of the film and $\lambda/4$ as a and b correspondingly the coefficients become $\mathbb{N}xx = 0$ and $\mathbb{N}yy = \frac{4t}{\lambda}$. For one of this $\frac{\lambda}{4}$ domains, using the expression for uniform resonance in the ellipsoid obtained in equation (2.14) we obtain an approximation for the resonance frequency:

$$\omega_{res} = \sqrt{\omega_H \left(\omega_H + \omega_M \frac{4t}{\lambda} \right)} \quad (2.30)$$

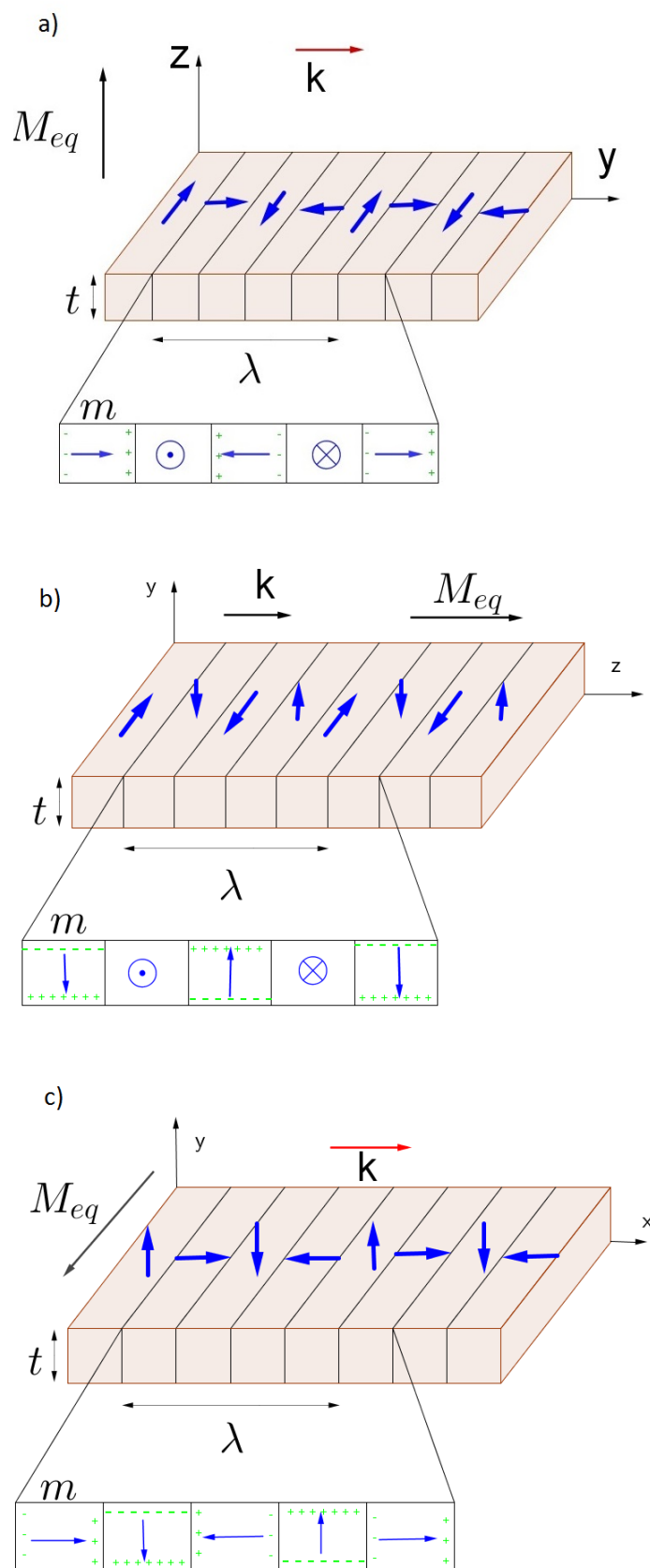


Figure 2.5: Diagrams for the propagation modes a) MsFVW b) MsBVW c) MsSW

or $\omega_{res} = \sqrt{\omega_H (\omega_H + \omega_M \frac{2kt}{\pi})}$. This expression reveals that the frequency depends on $k^{1/2}$, therefore the group velocity is different than zero. To obtain the exact dispersion relation, the magnetostatic potential $\psi(\vec{r}, \vec{k})$ is replaced in Maxwells boundary conditions at the top and bottom of the film, the potential is a propagative wave inside the film and an evanescent one outside. The solution of this problem for a metallic film was done first by Kalinikos in 1980 [6]; the exact dispersion relation for the MsFVW is:

$$\omega^2 = \omega_H \left(\omega_H + \omega_M \left(1 - \frac{1 - e^{-kt}}{kt} \right) \right) \quad (2.31)$$

The frequency expressed in the previous equation also satisfy the minimum and maximum value described in equation (2.27). Moreover, as seen in equation (2.30) the frequency increases as the k vector does so the group velocity is positive, the energy flux has the same direction as the propagation of the wave, that is the reason why it is a Forward volume wave.

This propagation mode is the one chosen for the development of the numerical study presented in this work.

Magnetostatic Backward Volume Wave The second propagation mode is called Magnetostatic Backward Volume Wave (MsBVW) and corresponds to the configuration shown in figure (2.5 b) where the magnetization is parallel to the wave vector and both lie parallel to the film. In this mode the “charges” are induced in upper and lower surfaces of the film. Therefore the demagnetizing coefficients are $N_{xx} = 0$ and $N_{yy} = 1 - \frac{4t}{\lambda}$. As before the resonance frequency is calculated by using the result for an ellipsoid in equation (2.14).

$$\omega_{res} = \sqrt{\omega_H \left(\omega_H + \omega_M \left(1 - \frac{4t}{\lambda} \right) \right)} \quad (2.32)$$

The latter expression shows that the frequency is a decreasing function of $k^{1/2}$. The group velocity ($v_g = \frac{d\omega}{dk}$) for this case is negative and the phase velocity ($v_\phi = \frac{\omega}{k}$) is positive, meaning that the energy flux goes against the phase propagation.

In 1960 Damon and Eshbach demonstrated that the exact dispersion relation for this mode is [22]:

$$\omega^2 = \omega_H \left(\omega_H + \omega_M \left(\frac{1 - e^{-k_z t}}{k_z t} \right) \right)$$

where k_z is the wave vector along the long axis of the film.

Magnetostatic Surface Wave The last mode corresponds to the configuration shown in figure (2.5 c), is called Magnetostatic Surface Wave. In this mode the magnetization and the wave vector both lie parallel to the film but are perpendicular between each other. In this mode the “charges” are induced in the wave’s planes for certain seg-

ments and on the surface of the film for the remaining ones as illustrated in figure (2.5 c). For this case the demagnetizing coefficients are $\mathbb{N}xx = \frac{4t}{\lambda}$ and $\mathbb{N}yy = 1 - \frac{4t}{\lambda}$ and the resonance frequency is:

$$\omega_{res} = \sqrt{\omega_H (\omega_H + \omega_M) + \omega_M^2 \frac{4t}{\lambda}} \quad (2.33)$$

In this case the group velocity is positive for that the frequency depends on $k^{1/2}$ so the energy flux goes in the same direction as the phase of the wave. Moreover, Damon and Eshbach also calculated the exact dispersion relation for this mode [22]:

$$\omega^2 = \left(\omega_H + \frac{\omega_M}{2} \right)^2 - \left(\frac{\omega_M}{2} \right)^2 e^{-2kt}$$

2.3 Phenomenological approach of damping

Up to this point we have assumed that all processes are ideal and have no energy losses, but in reality once the excitation disappears the magnetization relaxes to its equilibrium direction as its energy is redistributed into different damping mechanisms [3].

In order to understand phenomenologically for damping, Gilbert introduced into the equation of motion an additional viscous term proportional to the time derivative of the magnetization. In the case of small precession angles the equation is:

$$\frac{\partial \vec{M}}{\partial t} = -\gamma \mu_0 \vec{M} \times \vec{H}_{ef} + \frac{\alpha}{M_s^2} \vec{M} \times \frac{\partial \vec{M}}{\partial t} \quad (2.34)$$

where α is a dimensionless dissipative parameter. This process is similar to having assumed that there is a friction field $\frac{\alpha}{\gamma M_s^2} \left(\frac{\partial \vec{M}}{\partial t} \right)$ acting on the magnetization. This phenomenological expression satisfies the condition written in equation (2.2) that preserves the module of the magnetization. The latter expression can be linearized following the same process described in section 2.1.2, equation (2.5) becomes

$$i\omega \vec{m} = -\gamma \mu_0 \left(\vec{M}_{eq} \times \vec{h}(t) + \vec{m}(t) \times \vec{H}_{eq} \right) + i\omega \frac{\alpha}{M_s} \vec{M}_{eq} \times \vec{m} \quad (2.35)$$

The introduction of the Gilbert damping term is equivalent to the following substitution:

$$\omega_H \rightarrow \omega_H + i\alpha\omega$$

The form of the magnetization, for a uniform excitation, taking into account of energy loss [3] becomes:

$$\begin{aligned} m_x(t) &= \omega_M e^{-\alpha\omega_H t} \sin(\omega_H t) \\ m_y(t) &= -\omega_M e^{-\alpha\omega_H t} \cos(\omega_H t) \end{aligned} \quad (2.36)$$

This solution corresponds to a spherical spiral that decreases exponentially. Moreover,

due to the action of the friction in the system the magnetization responds resonantly not only to one frequency but to a range of them provoking a wide resonance peak. Therefore the presence of damping leads to a lorentzian imaginary and real part of χ :

$$\begin{aligned}\chi'_+ &= \text{Re}\{\chi_+\} = \frac{\gamma\mu_0 M_s (\gamma\mu_0 H_{eq} - \omega)}{(\gamma\mu_0 H_{eq} - \omega)^2 + \alpha^2 \omega^2} \\ \chi''_+ &= \text{Im}\{\chi_+\} = \frac{-\alpha\gamma\mu_0 M_s \omega}{(\gamma\mu_0 H_{eq} - \omega)^2 + \alpha^2 \omega^2}\end{aligned}\quad (2.37)$$

where the imaginary part of χ has a lorentzian form with a full width at half maximum $\Delta H = \frac{2\alpha\omega}{\gamma\mu_0}$ as seen on figure (2.6).

It is useful to define the frequency linewidth when observing an experiment that sweeps the frequency, for this purpose we will approximate $\frac{\Delta\omega}{\Delta H_{eq}} = \frac{\partial\omega}{\partial H_{eq}}$, using this expression into the dispersion relation written in equation (2.31) for the MsFVW mode we get:

$$\Delta\omega = 2\alpha\omega_{res} \quad (2.38)$$

From the frequency linewidth, we define a characteristic relaxation time $\tau = \frac{2}{\Delta\omega}$ and a characteristic attenuation length:

$$L_{att} = v_g \tau = \frac{v_g}{\alpha\omega} \quad (2.39)$$

In particular for Permalloy, typical attenuation lengths vary between $1 < L_{att} < 10 \mu m$.

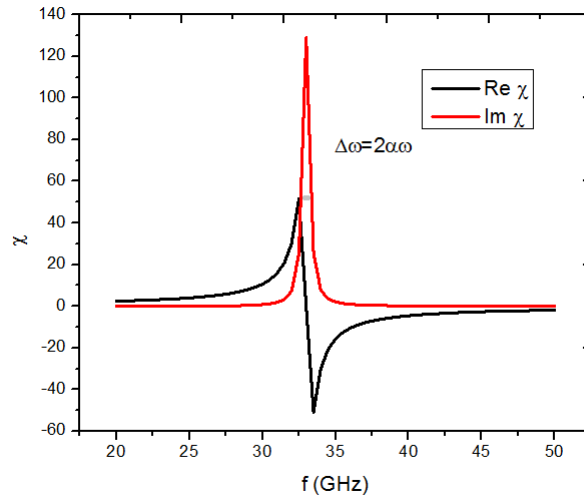


Figure 2.6: Real and imaginary parts of χ for $H_{eff} = 1,1 T$, $\alpha = 0,0075$ and $M_s = 1 T$

3 Propagating Spin wave Spectroscopy

We will now present one of the most common experimental techniques to excite and detect spin wave which is known as Propagating Spin-Wave Spectroscopy (PSWS) [8, 1]. Then we will present a model that translates the experimental technique with the physical quantities associated to spin waves.

3.1 Description of the technique

We will describe step by step the mechanism of excitation and detection of the spin waves in the PSWS technique. Figure (3.1) shows a sketch of the setup for the spectroscopy technique. The orange device is the sample, a ferromagnetic thin strip which is located on a probe station inside an electromagnet. The devices sketched in yellow are spin wave antenna which consists on shorted coplanar wave guides that can be folded into a meander shaped pattern. The antenna on the left is for excitation of the spin wave and the one in the right is for detecting the spin wave.

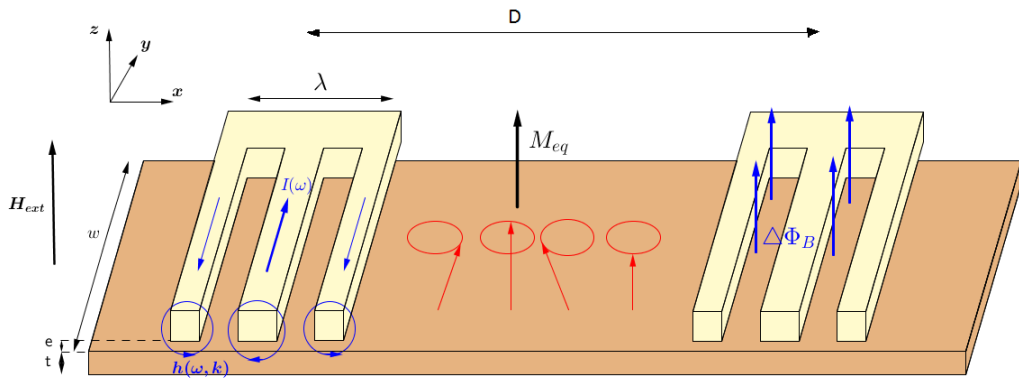


Figure 3.1: Experimental setup

The excitation antenna is usually connected to a Vector Network Analyzer (VNA) that injects a microwave current that generates a spatially periodic excitation field. This field will excite spin waves with majorital specific modes due to the shape of the antenna. The wavelength λ is roughly determined by the separation between ground planes. More exactly, the excitation spectrum is given by the Fourier transform of the antenna which we will cover later.

The ferromagnetic film is the media where spin waves propagate and generates a time dependent magnetic flux. The second antenna detects the spin wave through inductive coupling by measuring the induced voltage $V(\omega)$. In other words, we measure a change of inductance at the detection antenna due to the increase of magnetic flux associated with the spin wave traveling underneath.

The end of the detection antenna is connected to the second port of the VNA, which provides information on both phase and amplitude of the spin wave signal. The PSWS

is the technique of choice to study the propagation of spin wave as that it allows to select a specific wave vector through the dimension of the antenna, also it offers a high sensitivity with a threshold detection around the $10 fH$.

3.2 Spin wave transduction model

We study the spin wave transduction using a model developed initially by Emtage [11] and adapted more recently by Vlaminck et al [8] for spin wave propagation. It consists in a complete resolution of Maxwell equations in the geometry of the PSWS.

The calculation follows the three main steps of a spin wave transduction experiment.

1st step.- Production of a spatially resolved excitation field from the excitation antenna.

2nd step.- Generation of spin waves which propagate in the film.

3rd step.- Inductive detection at the second antenna.

3.2.1 Inductance of the antennas

The antennas that excite and detect the spin waves will be described using inductance. We will consider the self inductance of the exciting antenna when the same antenna excites and detects the spin wave and the mutual inductance between the exciting and detecting antenna when the wave propagates between the two of them.

First we will treat the self inductance of the antenna when it both excites the spin wave and detects it. In order to simplify the calculations we will assume that the antennas are infinitely thin and instead of working with the current we will work with the current linear density. We will also assume that the antenna is infinitely extended over the y axis so that we will be able to work with the inductance per unit of length \mathcal{L} , $\mathcal{L} = \frac{L}{w_y}$ where w_y is the width of the strip in the y axis and scale the amplitude of the signal with the strip width.

We will write the expression for the self inductance of the first antenna using the total complex power

$$L_{11} = w_y \mathcal{L}_{11} = \frac{P_{tot}}{i\omega I^2}$$

where

$$\mathcal{L}_{11} = \frac{1}{i\omega I^2} \int dx E_y(x, e, \omega) j_\epsilon(x, \omega)$$

$E_y(x, e, \omega)$ is the electric field induced by the spin wave excitation and the direct coupling (back emf) in the antenna. According to the theorem of Parseval, “the total energy contained in a waveform does not depend on its representation”; therefore we choose to work with the reciprocal space and integrate over the entire wave vector spectra. The self inductance transforms into

$$\mathcal{L}_{11}(\omega) = \frac{1}{i2\pi\omega I^2} \int_{-\infty}^{\infty} \tilde{E}_y(k, e, \omega) \tilde{j}_\epsilon(k, \omega) dk \quad (3.1)$$

where $\tilde{E}_y(k, e, \omega)$ is the Fourier transform of the induced electric field and $\tilde{j}_\epsilon(k, \omega)$ is the Fourier transform of the current density.

The mutual inductance in the second antenna is obtained by multiplying it by the integrand of the self inductance by a phase delay term which will propagate the spin wave.

$$\mathcal{L}_{21}(\omega) = \frac{1}{i2\pi\omega I^2} \int_0^\infty \tilde{E}_y(k, e, \omega) \tilde{j}_\epsilon(k, \omega) e^{ikD} dk \quad (3.2)$$

The distance between the antennas measured from center to center is D , then the phase delay has the form e^{-ikD} . The mutual induction only takes into account the waves that propagate to the right because the antenna cannot detect waves that travel to the left, therefore we must only integrate over wave vectors propagating to the right.

1st step.- Excitation field

The magnetic field generated by the antenna depends on the current that flows through it, for this we will work with a current distribution $\tilde{j}_\epsilon(k, \omega) e^{i(\omega t - kx)}$ to calculate the induced electric field. Figure (3.2) shows a sketch of the distribution of magnetic field and currents. Moreover, the film has a thickness t , and the distance between the film and the antenna e is called the spacer.

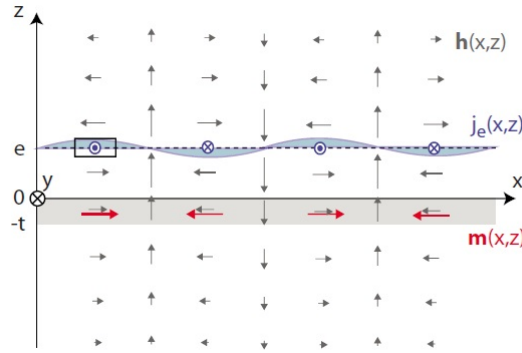


Figure 3.2: Vector field distribution of the magnetostatic field \vec{h} for a given Fourier component of the wave vector k . The distributions of linear current density j_ϵ and oscillating magnetization \vec{m} are sketched as arrows. [8]

Using ampere's law with a contour C as the one presented on figure (3.2), $\oint_C \vec{h} \cdot d\vec{l} = I_{enc}$ becomes:

$$h_x(k, e^+, \omega) - h_x(k, e^-, \omega) = j_\epsilon(k, \omega)$$

The corresponding Fourier transform of the latter equation is:

$$\tilde{h}_x(k, e^+, \omega) - \tilde{h}_x(k, e^-, \omega) = \tilde{j}_\epsilon(k, \omega) \quad (3.3)$$

2nd step.- Magnetic response

In order to express the magnetic response to an excitation field we will introduce the surface permeability μ_s , defined on the original formulation of Emtage [11]. The surface permeability μ_s is a dimensionless quantity defined as the ratio between the transverse induction $b_z(k, z, \omega)$ and the excitation field $h_x(k, z, \omega)$

$$\mu_s(k, z_0, \omega) = \lim_{z \rightarrow z_0} -i \frac{\tilde{b}_z(k, z, \omega)}{\mu_0 \tilde{h}_x(k, z, \omega)} \quad (3.4)$$

The relation between the surface permeability in two different position z_1 and z_2 for a MsFVW where the field is applied perpendicularly to the film is [1]:

$$\mu_s(z_1) = \frac{\mu_s(z_2) + (1 + \chi) \frac{\tanh(k(z_1 - z_2)\sqrt{1 + \chi})}{\sqrt{1 + \chi}}}{1 + \mu_s(z_2) \frac{\tanh(k(z_1 - z_2)\sqrt{1 + \chi})}{\sqrt{1 + \chi}}} \quad (3.5)$$

Using the magnetostatic potential, defined by $\vec{\nabla}(\psi) = \vec{h}$, in the semi spaces above and below the ferromagnetic film, we can show that ψ decays exponentially, $\psi_{e\pm}(x, y, z) \sim e^{\mp kz} e^{ikx}$; for this reason [8]:

$$\mu_s(k, \pm\infty) = \mp \frac{|k|}{k}$$

Therefore we will calculate in “ladder” at different heights using equation (3.5). In order to express the discontinuity of μ_s below and above the antenna. We want to establish this discontinuity of μ_s across the antenna. Therefore we obtain $\mu_s(e^-)$ starting from $z = -\infty$ and $\mu_s(e^+)$ starting for $z = +\infty$. We will iterate first between infinity and the bottom of the field, $\mu_s(k, -\infty) = \mu_s(k, -t, \omega)$, then we will access the film to obtain $\mu_s(k, 0, \omega)$ (permeability at the top of the film), using $\mu_s(k, 0, \omega)$ we get $\mu_s(k, e^-, \omega)$ (at the bottom of the antenna). Finally, to establish the discontinuity across the antenna we iterate one last time $\mu_s(k, e^+, \omega) = \mu_s(k, +\infty)$.

The discontinuity in the magnetic field described in equation (3.3) can be rewritten using the upper and lower limits of the surface permeability.

$$\mu_0 \tilde{j}_e(k, e, \omega) = -i \tilde{b}_z(k, e, \omega) \left(\frac{1}{\mu_s(k, e^+, \omega)} - \frac{1}{\mu_s(k, e^-, \omega)} \right) \quad (3.6)$$

3rd step.- Induced electric field

We now establish the relation between the magnetic magnetic flux variation due to the spin wave and electric field induced in the antenna. Using Maxwell-Faraday equation:

$$\begin{aligned} \vec{\nabla} \times \vec{E} &= -\frac{d\vec{b}}{dt} \\ -\frac{\partial E_y}{\partial z} \hat{x} + \frac{\partial E_x}{\partial x} \hat{z} &= -i\omega \vec{b} \end{aligned}$$

where the first term is equal to zero. Since both electric and magnetic field have a

$e^{i(\omega t - kx)}$ factor, the latter equation becomes

$$E_y(k, z, \omega) \hat{z} = -\frac{\omega}{k} b_z(k, z, \omega) \hat{z}$$

by taking the Fourier transform

$$\tilde{E}_y(k, z, \omega) = -\frac{\omega}{k} \tilde{b}_z(k, z, \omega) \quad (3.7)$$

Using the previous equations, we can write the electric field of the antennas as:

$$\tilde{E}_y(k, e, \omega) = i\mu_0 \left(\frac{\omega}{k}\right) \frac{\tilde{j}_\epsilon(k, \omega)}{\frac{1}{\mu_s(k, e^+, \omega)} - \frac{1}{\mu_s(k, e^-, \omega)}} \quad (3.8)$$

Finally, by replacing the induced fields into the inductances of the antennas we obtain:

$$\mathcal{L}_{11} = \frac{\mu_0}{2\pi} \int_{-\infty}^{+\infty} \frac{1}{k} \left| \frac{\tilde{j}_\epsilon(k, \omega)}{I} \right|^2 \frac{1}{\frac{1}{\mu_s(k, e^+, \omega)} - \frac{1}{\mu_s(k, e^-, \omega)}} dk \quad (3.9)$$

$$\mathcal{L}_{21} = \frac{\mu_0}{2\pi} \int_0^{+\infty} \frac{e^{-ikD}}{k} \left| \frac{\tilde{j}_\epsilon(k, \omega)}{I} \right|^2 \frac{1}{\frac{1}{\mu_s(k, e^+, \omega)} - \frac{1}{\mu_s(k, e^-, \omega)}} dk \quad (3.10)$$

These are the expressions that will be numerically integrated.

3.3 Fourier Transform of the antenna

We will now obtain the Fourier transform of the antenna in order to analyze how does the repeating pattern affects the excited wave vector spectrum.

Figure (3.3 b) shows the current density distribution. The device has been manufactured with dimensions that make the current distribution as close as possible to a sinusoidal. In order to work with the antenna we must analyze the repeating pattern as sketched in figure (3.3 a). The Fourier transform of the pattern normalized by the current I is:

$$\frac{\tilde{j}_{pattern}(k)}{I} = \frac{\sin\left(\frac{kl_g}{2}\right)}{\frac{kl_g}{2}} - 2\cos\left(\frac{k(l_g + l_p + 2l_1)}{2}\right) \frac{\sin\left(\frac{kl_p}{2}\right)}{\frac{kl_p}{2}} \quad (3.11)$$

The transform of the total antenna is obtained by translating and inverting the pattern, the distance between the center of one pattern to another is $L_{pattern} = l_g + l_{o2} + 2l_p + 2l_{o1}$, we must translate and invert the pattern a distance $L_{pattern}$. The Fourier transform of a three meander antenna is:

$$\frac{\tilde{j}_\epsilon(k)}{I} = \frac{\tilde{j}_{pattern}(k)}{I} (1 - 2\cos(kL_{motif})) \quad (3.12)$$

As seen in figure (3.3 c) the periodicity of the meander allows to reduce the width of the excited wave vector spectrum.

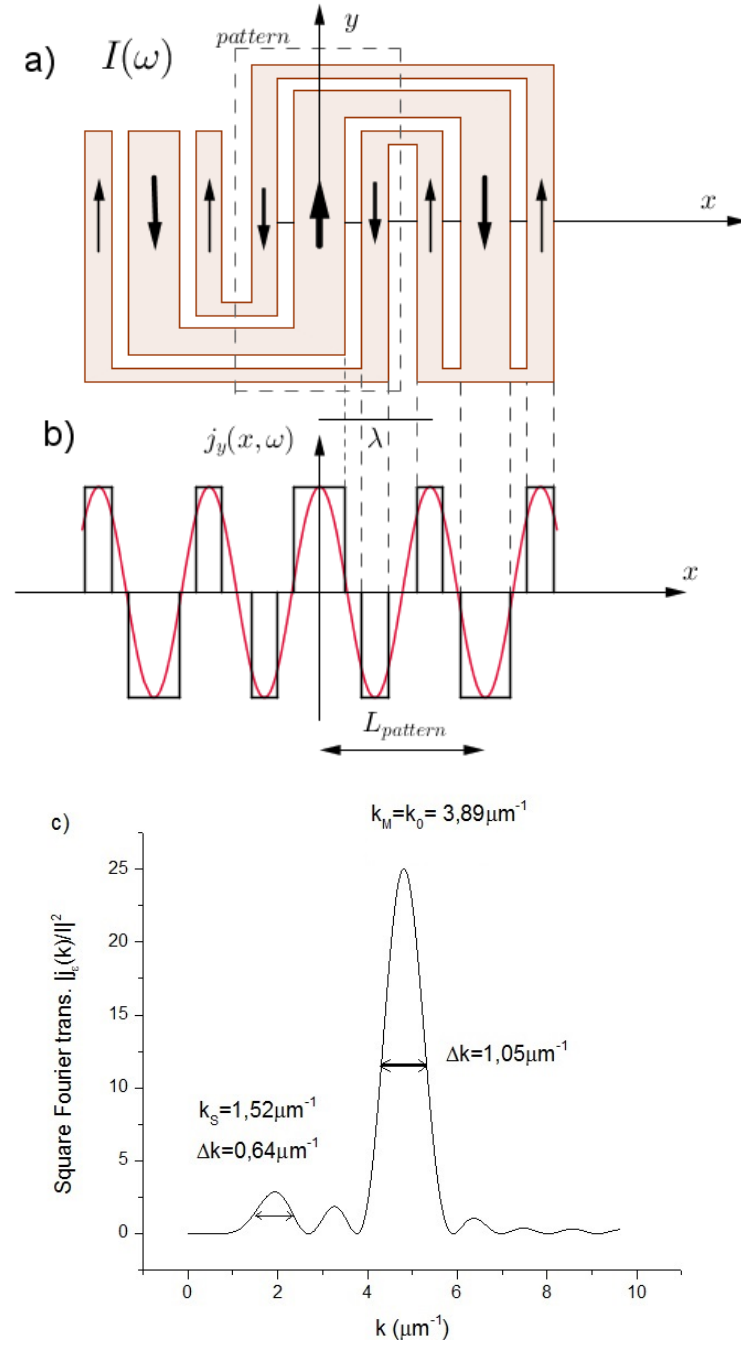


Figure 3.3: Typical antenna and current distribution (a) Meander shaped pattern short circuited at the end. (b) Current distribution. (c) Square of the Fourier transform of an antenna with dimensions $l_g = 675 \text{ nm}$, $l_{o2} = 475 \text{ nm}$, $l_p = 340 \text{ nm}$, and $l_{o1} = 300 \text{ nm}$. The main peak, $k_M = 3,86 \mu\text{m}^{-1}$ has a full width at half maximum $\Delta k = 1,05 \mu\text{m}^{-1}$, and the secondary peak $k_S = 1,52 \mu\text{m}^{-1}$ has a $\Delta k = 0,648 \mu\text{m}^{-1}$.

4 Simulation of the MsFVW

We will now present the simulation of the model which emulates the results that could be obtained during a propagating spin wave spectroscopy experiment for a magnetostatic forward volume wave in Permalloy. The simulation consists on generating spectra by numerical integration for the mutual inductance by sweeping frequency in a very similar manner to a real measurement with a Vector Network Analyzer (VNA). We will then compare the spin wave signal with the sensitivity of a real VNA in order to estimate the maximum distance over which we can propagate spin waves in a broad spectrum of frequency varying between 2 GHz and 30 GHz , and in wave vector varying between $0,5\ \mu\text{m}$ and $12,5\ \mu\text{m}^{-1}$ which correspond to an interesting scale for miniaturized electronic devices.

The main objective of this work is to establish the maximum propagation distance of a MsFVW as a function of the wave vector and the frequency in a thin Permalloy film. First we will analyze several spin wave spectra to verify the attenuation of the intensity with the separation D , and verify the dispersion relation for the MsFVW mode in order to validate the model.

All results presented in this section were obtained using a three meander antenna and a Permalloy sample, Permalloy is a soft material ($H_c \approx 1\text{ Oe}$) that has a microwave loss and almost no magnetocrystalline anisotropy [18]. The values chosen for the wave vector correspond to an antenna that can be fabricated and has been studied experimentally [1]. In order to cover the entire wave vector spectrum the antenna will be scaled to fit the corresponding λ . We fix the magnetic external field between 1 T and 2 T . The magnetic parameters for Permalloy are: damping coefficient $\alpha = 0,0075$, a gyromagnetic ratio $\gamma = 30\text{ GHz T}^{-1}$, and saturation magnetization $\mu_0 M_s = 1\text{ T}$. Moreover, we will fix the width of the strip at $w = 1\ \mu\text{m}$, the spacer between the antenna and the film as $e = 100\text{ nm}$, its thickness at $t = 20\text{ nm}$, and give all results per unit of width in μm^{-1} .

Moreover, to study the maximum propagation distance an optimization recursive algorithm was implemented. The generation of data is considered for a distance D between antennas and a wave vector k_0 defined by the size of the antenna. The algorithm has 3 steps:

Step 1.- A first spectra generation is performed to obtain the initial values for maximum inductance and propagation distance when antennas are very close.

Step 2.- A recursive function receives the initial values and compares them to $I_{max} = Ae^{-D/L_{att}}$ in order get a value for the initial constant A . Then, the minimum value of the inductance is replaced into the previous equation to obtain a value of D which will correspond to a tentative maximum propagation distance to an intensity of 1 fH .

Step 3.- The function generates spectra using the tentative attenuation length, then the function calls itself using this values.

The function only stops when the maximum value of the inductance is the same as

the one set for the sensitivity (with an error allowed interval) and returns the value of the maximum propagation distance.

4.1 Self inductance inductance spectra

First we will discuss some fundamental properties of MsFVW at reflexion, spectroscopy in reflexion consists on measuring the self inductance of the exciting antenna. Figures (4.1 a and c) show 2 graphs of inductance in reflexion for $k_M = 4,83 \mu m^{-1}$ and $k_M = 10,5 \mu m^{-1}$ at $H_{ext} = 1,1 T$. The graphs shows two separate peaks of resonance corresponding to the signature of the excitation spectra of the antenna (figure 3.3 c). Figures (4.1 b and d) show the reflexion spectra for both wave vectors correspondingly at $H_{ext} = 1,42 T$. For graphs (a) and (b), the main peak corresponds to $k_0 = 4,83 \mu m^{-1}$ and the secondary to $k_S = 2 \mu m^{-1}$. The width of the main peak increases with the magnetic field; for $H = 1,1 T$ the full width at half maximum is $\Delta f_1 = 0,13 GHz$ and for $H = 1,42 T$ is $\Delta f_1 = 0,27 GHz$.

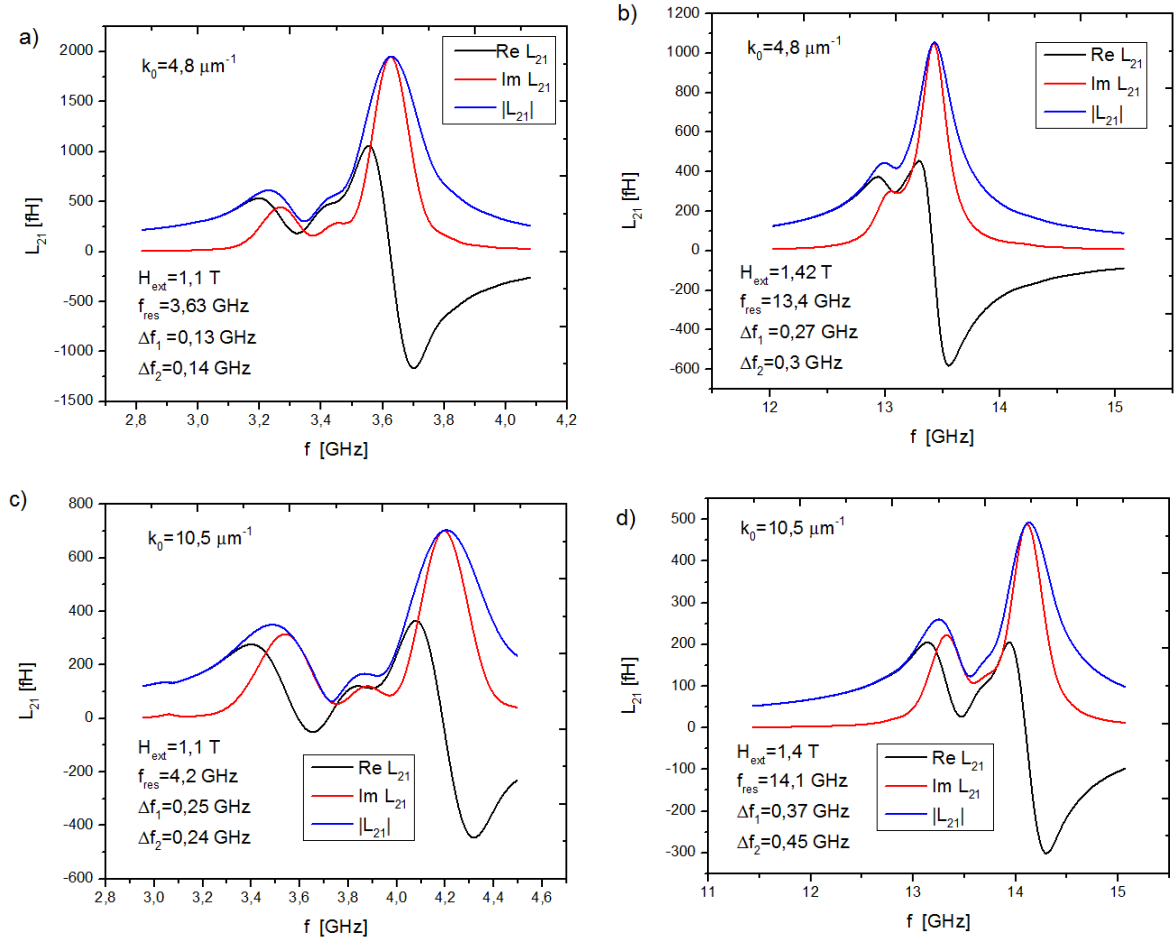


Figure 4.1: Spectra generated in Reflexion. a) $k_0 = 4,83 \mu m^{-1}$ at $H = 1,1 T$. b) $k_0 = 4,83 \mu m^{-1}$ at $H = 1,42 T$. c) $k_0 = 10,5 \mu m^{-1}$ at $H = 1,1 T$. d) $k_0 = 10,5 \mu m^{-1}$ at $H = 1,42 T$.

When examining figure (4.1 b) we observe that the resonance peaks appear to be closer to each other as the resonance frequency increases. Although they seem to be closer they are not, the peaks are separated $0,5 GHz$ in both cases and they seem closer because both of them are broader. Figure (4.2 b) shows the resonance frequency of both principal and secondary wave vectors for different magnetic fields; the difference between the resonance frequency of both wave vectors at $H = 1,1 T$ is $0,5 GHz$ and at $H = 1,42 T$ is $0,48 GHz$.

Now we will quickly examine the dispersion relation as a function of the wave vector and the frequency, presented in equation (2.31) for the MsFVW mode; it is plotted in figure (4.2) using a simulation. When examining the dispersion relation, we can remark that the resonance frequency increases with both the external field and the wave vector. Figure (4.2 b) corresponds to two sections of the 3D graph with constant field $H = 1,1 T$ and $H = 1,42 T$, that show a non linear dependence of the resonance frequency with the k vector. Also, figure (4.2 c) is a graph for two constant wave vectors, $k_0 = 4,83 \mu m^{-1}$ and $k_S = 2 \mu m^{-1}$, which shows that the frequency dependence with the field is almost linear. According to the Kalinikos dispersion relation, the frequency is proportional to the square root of a quadratic polynomial of $\omega_H = \gamma \mu_0 H$. Also, the resonance frequency increases much rapidly with the external field than it does with the wave vector.

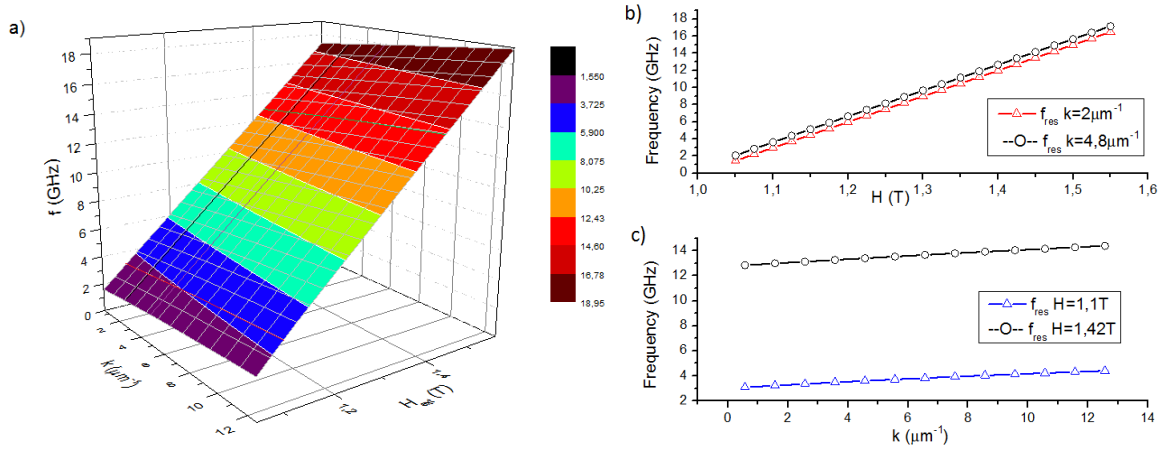


Figure 4.2: A) 3D plot $\omega(k, H)$. b) Section for constant wave vector, $k_0 = 4,83 \mu m^{-1}$ purple line in (a), $k_0 = 2 \mu m^{-1}$ black line in (a). c) Section for constant magnetic field, $H = 1,1 T$ red line in (a), $H = 1,42 T$ green in (a).

The resonance peaks get broader as the field increases because of the damping processes, as described before $\Delta f = 2\alpha f_{res}$. Also we must consider the extrinsic contribution due to the non monochromatic excitation, $\Delta f_{extrinsic} = v_g \Delta k / 2\pi$ [1]. This contribution to the peak broadening is presented on figure (4.3 a); the graph shows the full width at half maximum for $k_0 = 4,8 \mu m^{-1}$ at different frequencies. The data plotted in the graph shows a linear dependence of the linewidth with frequency, with a slope of $0,017$ and an offset value of $0,054 GHz$. Since the linewidth depends on the intrinsic

and extrinsic contributions and the intrinsic contribution is $2\alpha f$, the slope of the fit done should match 2α , the porcentual error is 13,3%; also the offset value corresponds to the extrinsic contribution. It is interesting to observe that the slope is not rigorously equal to 2α as it would be in the case of a experiment with uniform excitation ($k = 0$). Moreover, the slope is higher than the expected one because the extrinsic term in the latter expression depends on the group velocity, which increases with the frequency. Figure (4.3 a) also shows the width of the main resonance peak of graph (a) for different frequencies. This same phenomena is appreciated when comparing figures (4.1 c and d), for this graphs the main peak is $k_0 = 10,5 \mu\text{m}^{-1}$ and the secondary peak is $k_S = 3,5 \mu\text{m}^{-1}$. The same analysis performed and presented on figure (4.3 b), the slope of the width of the main resonance peak is 0,015 which gives a porcentual error of 2,26%.

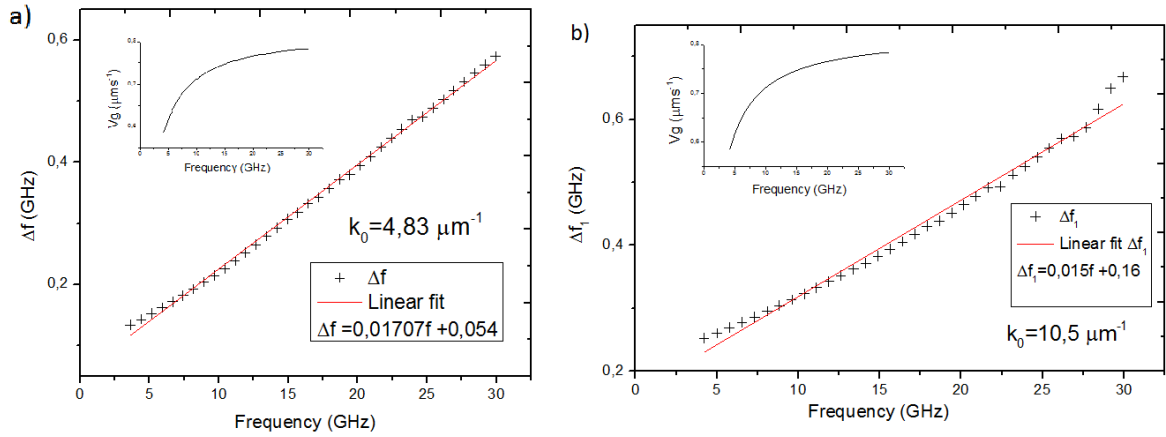


Figure 4.3: Frequency linewidth for main and secondary peaks at $H = 1,1 T$. a) $k_0 = 4,83 \mu\text{m}^{-1}$. b) $k_0 = 10,5 \mu\text{m}^{-1}$.

4.2 Mutual inductance spectra

Figure (4.4a-d) displays the inductance in transmission for the same values of wave vector as the cases presented in reflexion. The graphs show how the initial perturbation transforms into an oscillation, where the real and imaginary part of the induction have a $\frac{\pi}{2}$ phase difference. The phase difference corresponds to the excitation spectra $\delta\phi = \delta k L$, an entire oscillation is $\Delta\phi = 2\pi$ so $2\pi = \Delta k L$. The linewidth Δf appears because of the propagation of this phase difference, therefore $\Delta f = \frac{v_g}{L} = \frac{v_g \Delta k}{2\pi}$. The multiple wave vector excited initially accumulate phase delay during the propagation; the greater distance the wave propagates, the more oscillations appear. Also, the graphs show that the intensity of the signal decreases significantly with distance due to the damping processes. The relative height of the peak varies as the wave propagates, as seen in graphs (a-d) of figure (4.4) the secondary peak, which has a lower wave vector, tends to reduce its intensity values less rapidly. Moreover, by comparing figure (4.4 a) with (4.4 d) we note that the shape of the modulus of the inductance in transmission

resembles the one in reflexion . The characteristic peaks of the Fourier transform are still displayed in transmission but they have different relative heights. The shape of the inductance in reflexion acts as an envelope only for the widths of the peaks.

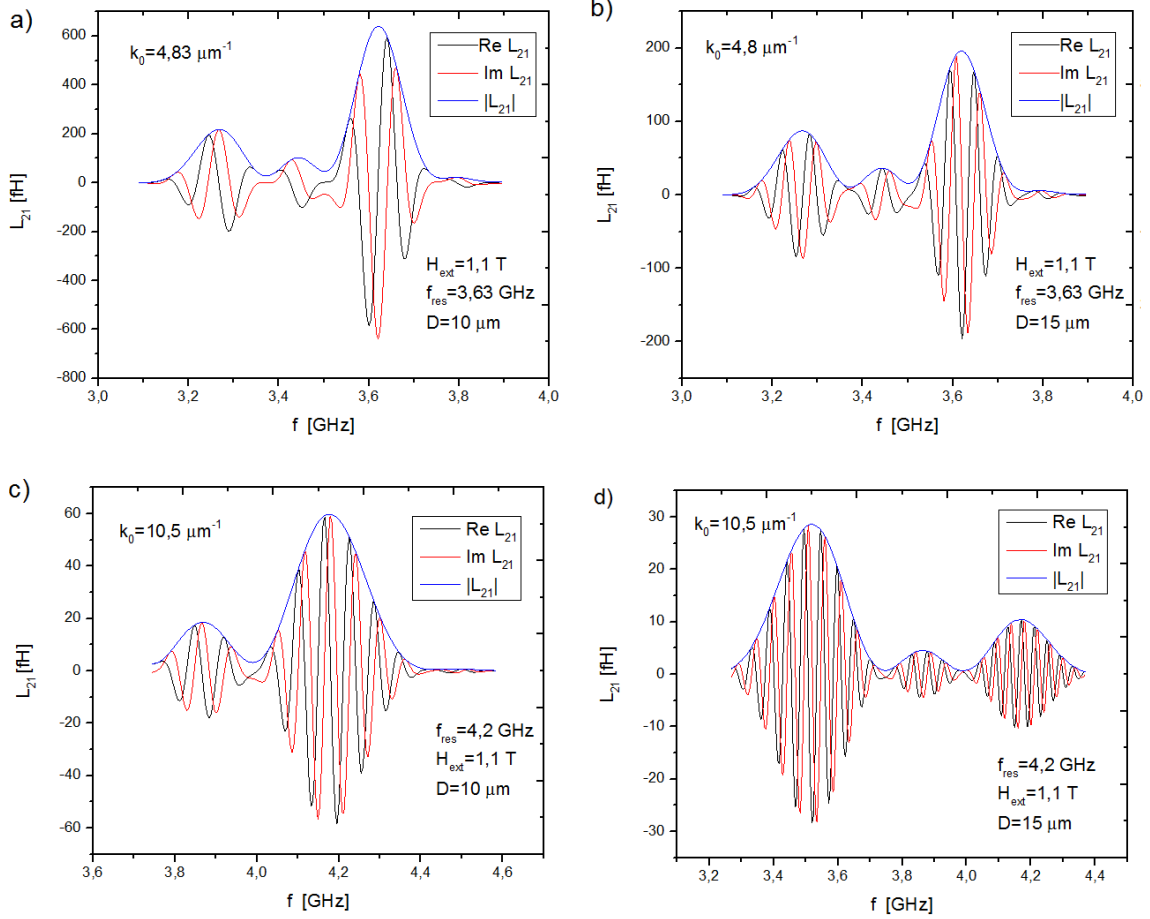


Figure 4.4: Spectra generated for Inductance in transmission at $H = 1,1 \text{ T}$ a) $k_0 = 4,83 \mu\text{m}^{-1}$ with $D = 10 \mu\text{m}$ b) $k_0 = 4,83 \mu\text{m}^{-1}$ with $D = 15 \mu\text{m}$ c) $k_0 = 10,5 \mu\text{m}^{-1}$ with $D = 10 \mu\text{m}$ d) $k_0 = 10,5 \mu\text{m}^{-1}$ with $D = 15 \mu\text{m}$.

4.2.1 Attenuation length

Figure (4.5) a) shows that the attenuation length of the propagated wave decreases as the external field increases, this phenomena occurs because the expected propagation is inversely proportional to the resonance frequency and the frequency increases along with the field. The highlighted particularity can be interpreted as if the magnetization is stiffer as the field increases, more energy is needed in order to start precession causing resonance to be at a higher frequency.

Additionally, using plots for constant wave vector and constant field we will compare the attenuation length obtained through the simulation with the expected one from equation (2.39).

An evidence of the damping process discussed before is presented in figure (4.5). This graph shows the decrease of intensity of the maximum value of the mutual inductance's main peak during propagation for an increasing magnetic field for one wave vector ($k_0 = 9 \mu m^{-1}$). Figures (4.5b and c) show examples of the decrease of intensity for an increasing distance for different magnetic fields, in each graph an exponential fit has been done in order to calculate the expected attenuation length using equation (2.39). The porcentual error for $H = 1,1 T$ is 2,9% and is 0,08% for $H = 1,5 T$. It is notable that in all cases the actual attenuation length is smaller than the calculated one.

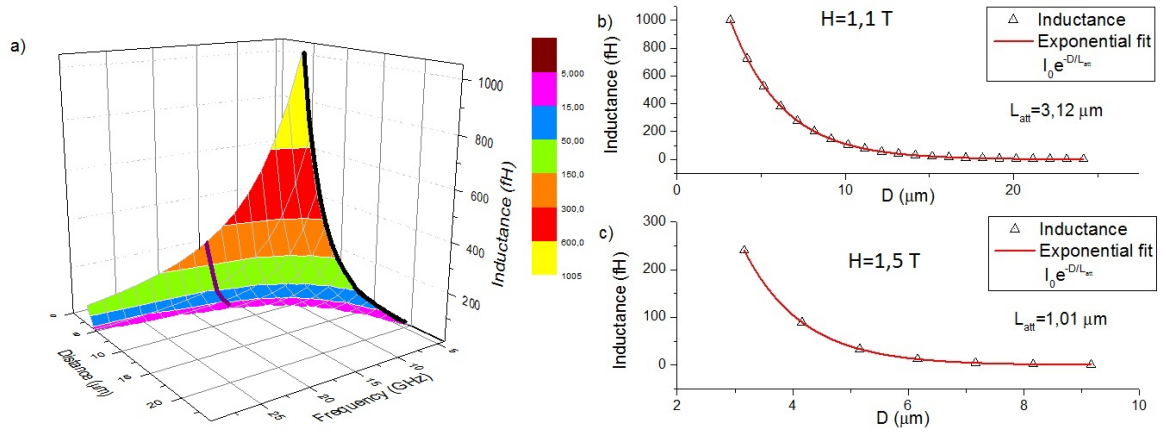


Figure 4.5: a) Propagation for an increasing field at $k_0 = 9 \mu m^{-1}$. b) Peak value of inductance at 1,1 T 4,07 GHz, black line of (a) graph, expected attenuation length 3,216 μm and fitted 3,121 μm c) Inductance through propagation at 1,5 T with resonance at 16,2 GHz, purple line of (a) graph, expected attenuation length 1,015 μm and fitted 1,016 μm .

When plotting the inductance as a function of distance and wave vector, as in figure (4.6 a), we observe that as the wave vector increases the attenuation length decreases due to the increase on the resonance frequency; according to equation (2.39) the attenuation length is inversily proportional to the resonance frequency. For the extreme value of the graph, $k_0 = 12,5 \mu m^{-1}$ the propagation distance is 10,2 μm and for $k_0 = 2 \mu m^{-1}$, $d = 30 \mu m$. Figures (4.6 b and c) are sections that present the relation between the intensity of the signal and the distance for 4,5 μm^{-1} and 11,5 μm^{-1} correspondingly. As before, an exponential fit was performed in order to obtain the attenuation length, the error between the fitted value and the expected one are 0,28% and 0,93% respectively.

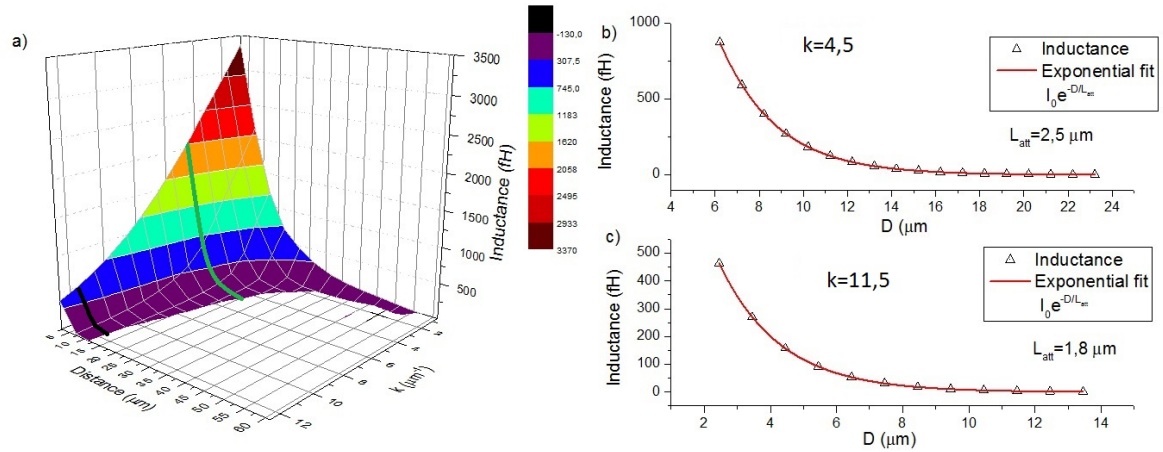


Figure 4.6: Decrease of intensity in propagation for different wave vectors. a) 3D plot at $H_{ext} = 1,2 T$. b) Inductance through propagation for $k_0 = 4,5 \mu m^{-1}$, green line in graph (a), the attenuation length expected is $2,576 \mu m$ and the fitted one is $2,568 \mu m$; resonance is at $6,63 GHz$. c) Inductance through propagation for $k_0 = 11,5 \mu m^{-1}$, black line in graph (a), the expected attenuation length is $1,868 \mu m^{-1}$ and the fitted one is $1,851 \mu m^{-1}$, resonance frequency is at $7,43 GHz$.

4.3 Determination of the maximum propagation length

Finally, we now turn to the study of the maximum propagation distance for a MsFVW following the sensitivity threshold of a VNA. We generate series of spectra covering a wave vector range $[1 \dots 12,5] \mu m^{-1}$, and a frequency spectrum of $[5 \dots 20] GHz$ generating various particular distances between antennas until we reach a limiting value of $10 fH \pm 0,05$. The minimum value of the intensity was set by taking into consideration that the detective threshold using a VNA is around $50 fH$ [8, 13]. The value of $10 fH$ can be achieved experimentally by averaging dynamically a large number of repetitions (typically, the noise signal decreases by \sqrt{N} where N is the number of repetitions). Since this sensitivity is experimentally hard to achieve it is a good cut-off lower limit for the simulation.

Figure (4.7) shows the main result of this work, a 3D representation of the maximum propagation distance as a function of the wave vector and the resonance frequency. Values of the maximum distance for the wave vector $k_0 = 12,5 \mu m^{-1}$ (the high wave vector limit) with a frequency of $5 GHz$ range from $9 \mu m$ to $4 \mu m$ at $20 GHz$ and for the low wave vector limit, $k_0 = 1 \mu m^{-1}$, maximum propagation distance ranges from $31 \mu m$ at $5 GHz$ to $21 \mu m$ at $20 GHz$. Moreover, the maximum propagation distance decreases rapidly as both frequency and wave vector increase. In particular, the maximum propagation distance decreases more rapidly with the wave vector than it does with the increasing of the field.

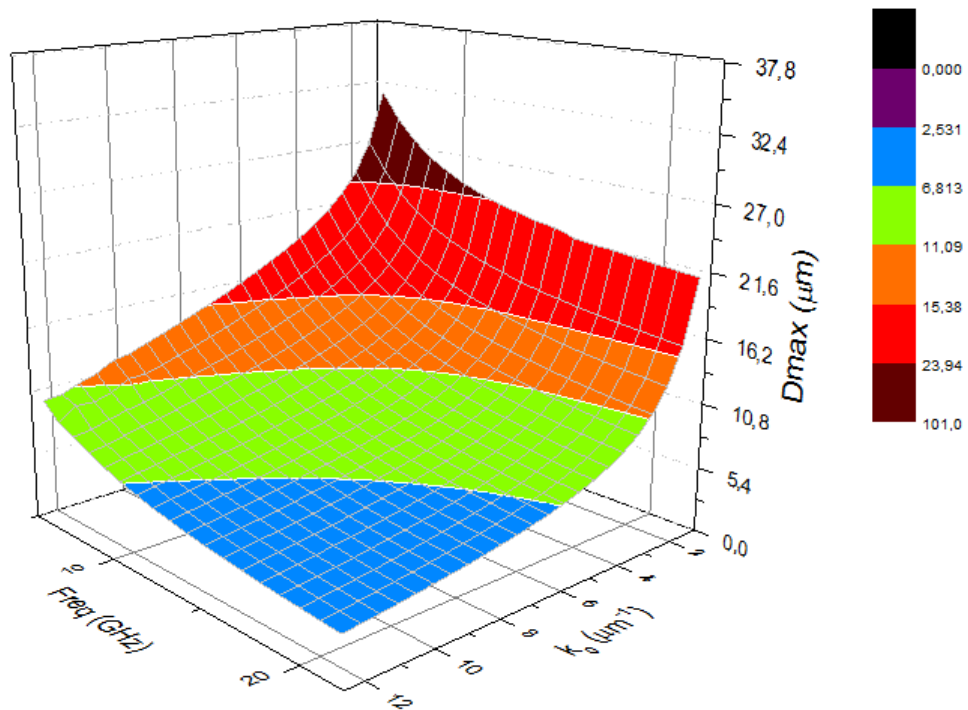


Figure 4.7: Maximum propagation distance for MsFVW in Permalloy, for a broad range of wave vector $k = [1 \dots 12, 5] \mu\text{m}^{-1}$ and frequency $f = [5 \dots 20] \text{GHz}$

5 Conclusions

In this work we have presented an electromagnetic model to describe the propagation of spin waves in a thin film in the magnetostatic regime. This model is a close adaptation of the propagation spin wave spectroscopy technique. This technique constitutes at this present time one of the most sensitive techniques to propagate coherent spin waves. We implemented this model aiming to explore the maximum propagation length of the magnetostatic forward volume wave (when the magnetization is perpendicular to the film and the wave vector lies on the films principal direction) for a $1 \mu m$ width strip of Permalloy. We estimated the maximum propagation distance of a spin wave by simulating the mutual inductance spectra with a detection threshold of $10 fH$ which corresponds to the detection sensitivity limit of the vector network analyzer. We were able to estimate the wave propagation length by comparing the intensity of the spin wave spectra with the detection threshold for a broad range of wave vector $k = [1 \dots 12,5] \mu m^{-1}$ and frequency $f = [5 \dots 20] GHz$. We observe a rapid decay of the maximum separation distance of a pair of antenna. For a wave vector of $1 \mu m^{-1}$ at $5 GHz$ the maximum propagation distance is $31 \mu m$ and for $12,5 \mu m^{-1}$ at $5 GHz$ is $9,5 \mu m$.

The optimization routine developed in this work to estimate the maximum propagation distance on the wave vector and frequency spectrum can now be implemented for other materials and other magnetostatic wave modes. This work serves as a reference for optimizing design of experimental devices implemented in Magnetostatic forward volume waves.

References

- [1] Vlaminck, V. (2008). *Décalage Doppler d'onde de spin induit par un courant électrique*. (Thèse de doctorat de l'Université Louis Pasteur).
- [2] Blundell, S. (2001). *Magnetism in Condensed Matter*. Oxford Master Series in Condensed Matter Physics.
- [3] Stancil, D. (1993). *Theory of Magnetostatic Waves*. New York: Springer Verlag. DOI: 10.1007/978-1-4613-9338-2
- [4] Gurevich, A. and Melkov, G. (1996). *Magnetization Oscillations and Waves*. Boca Raton: CRC Press
- [5] Coey, J. (2010). *Magnetism and Magnetic Materials*. New York: Cambridge University Press.
- [6] Kalinikos, B. (1981). Spectrum and Linear Excitation of Spin Waves in Ferromagnetic Films. *Soviet Physics Journal*. 24(8) 718-731
- [7] Bailleul, M. (2002). *Propagation et confinement d'ondes de spin dans les microstructures magnétiques*. (Thèse de doctorat de l'École Polytechnique).
- [8] Vlaminck, V. and Bailleul, M. (2010). Spin-wave transduction at the submicrometer scale: Experiment and modeling. *Physical Review B*. 81(014425). 1-13. DOI: 10.1103/PhysRevB.81.014425
- [9] Vlaminck, V. and Bailleul, M. (2008). Current-Induced Spin-Wave Doppler Shift. *Science* 322 (5900). 410-413. DOI: 10.1126/science.1162843
- [10] Landau, L. and Lifshitz, E. (1935). On the theory of the dispersion of magnetic permeability in ferromagnetic bodies. *Phys. Zeitsch. der Sow*, 8. 153–169
- [11] Emtage, P.R. (1978). Interaction of magnetostatic waves with a current. *Journal of Applied Physics*. 49(4475). DOI: <http://dx.doi.org/10.1063/1.325452>
- [12] Kruglyak, V., Demokritov, S. and Grundler, D. (2010). Magnonics. *Journal of Physics D: Applied Physics*, 43 (26).
- [13] Keysight Technologies. *Network Analyzer Selection Guide*. Recovered from: <http://literature.cdn.keysight.com/litweb/pdf/5989-7603EN.pdf?id=1405173>
- [14] Tamaru, S., Bain, J., van de Veerdonk, J., Crawford, T., Covington, M. and Kryder, M. (2004). Measurement of magnetostatic mode excitation and relaxation in Permalloy films using scanning Kerr imaging. *Physical Review B*. 70(104416). DOI: 10.1103/PhysRevB.70.104416

- [15] Khitun, A., Bao, M. and Wang, K. (2008). Spin Wave Magnetic NanoFabric: A New Approach to Spin-Based Logic Circuitry. *IEEE Transactions on Magnetics*. 44(9). 2141-2152. DOI: 10.1109/TMAG.2008.2000812
- [16] Kostylev, M., Serga, A., Schneider, T., Leven, B. and Hillebrands, B. (2005). Spin-wave logical gates. *Applied Physics Letters*. 87(153501). DOI: <http://dx.doi.org/10.1063/1.2089147>
- [17] Abo, G., Hong, YK., Park, J., Lee, J., Lee, W. and Choi, BC. (2013). Definition of Magnetic Exchange Length. *IEEE Transactions on Magnetics*, 49(8), 4937-4939. DOI: 10.1109/TMAG.2013.2258028
- [18] Kin Ha, J., Hertel, R. and Kirschner, J. (2003). Micromagnetic study of magnetic configurations in submicron Permalloy disks. *Physical Review B*. 67(224432). DOI: 10.1103/PhysRevB.67.224432
- [19] Schneider, T., Serga, A., Leven, B. and Hillebrands, B. (2008). Realization of spin-wave logic gates. *Applied Physics Letters*, 92(022505). DOI: 10.1063/1.2834714
- [20] Lee, KS. and Kim, SK. (2008). Conceptual design of spin wave logic gates based on a Mach-Zehnder-type spin wave interferometer for universal logic functions. *Journal of Applied Physics*, 104(053909),1. DOI: 10.1063/1.2975235
- [21] Smolenski, G. and Chupis, I. (1982). Ferroelectromagnets. *Soviet Physics - Uspekhi*. 25(7). 475-93.
- [22] Damon, R. and Eshbach J. (1960). Surface magnetostatic modes and surface spin waves. *Physical Review*, 118(1208).